ERDC TR-22-22

US Army Corps
of Engineers®
Engineer Research and
Development Center

ERDC
ENGINEER RESEARCH & DEVELOPMENT CENTER

Extreme Terrain Research

Meteorological Influences of a Major Dust Storm in Southwest Asia during July–August 2018

Ross E. Alter, Sandra L. LeGrand, Freddie D. Spates, William D. Ledbetter, Sherman D. Minnigan, John W. Thompson, Kindra I. Carter, and Phillip D. Elliott

November 2022

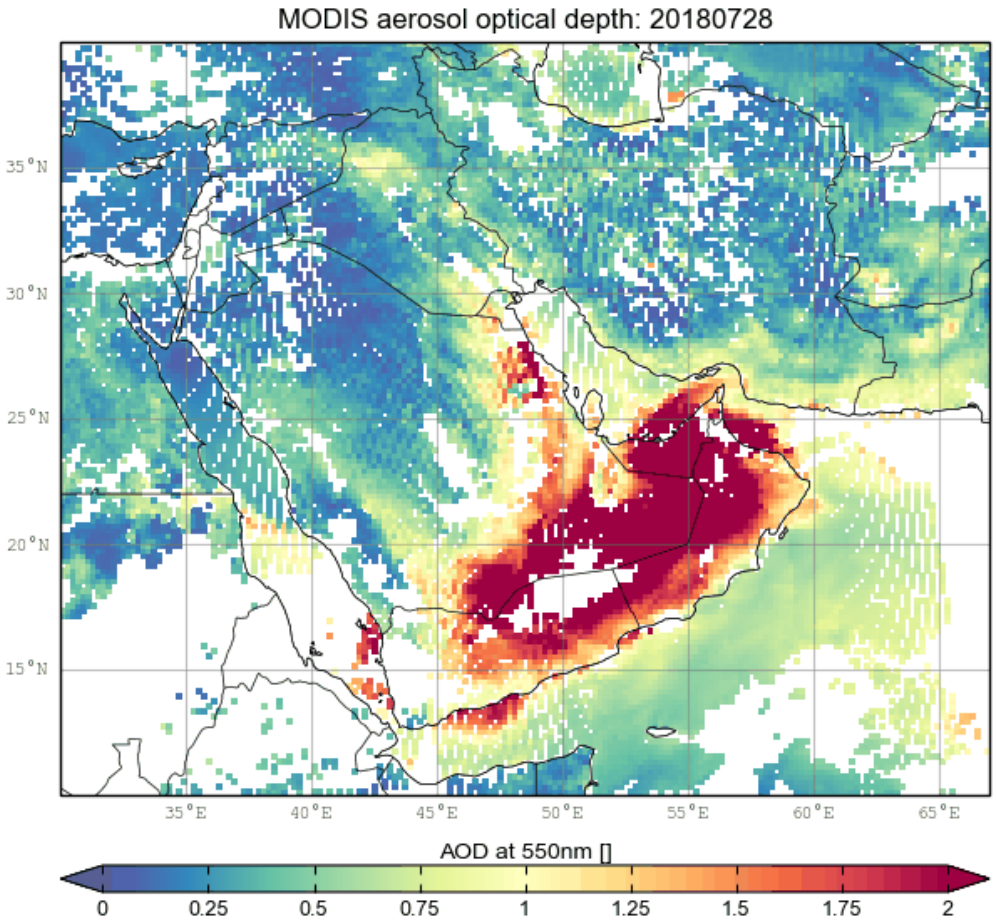

Engineer Research and Development Center

The US Army Engineer Research and Development Center (ERDC) solves the nation's toughest engineering and environmental challenges. ERDC develops innovative solutions in civil and military engineering, geospatial sciences, water resources, and environmental sciences for the Army, the Department of Defense, civilian agencies, and our nation's public good. Find out more at www.erdc.usace.army.mil.

To search for other technical reports published by ERDC, visit the ERDC online library at https://erdclibrary.on.worldcat.org/discovery.

ERDC TR-22-22
November 2022

Meteorological Influences of a Major Dust Storm in Southwest Asia during July–August 2018

Ross E. Alter

US Army Engineer Research and Development Center (ERDC)
Cold Regions Research and Engineering Laboratory (CRREL)
72 Lyme Road
Hanover, NH 03755

Sandra L. LeGrand

US Army Engineer Research and Development Center (ERDC)
Geospatial Research Laboratory (GRL)
7701 Telegraph Road
Alexandria, VA 22315-3864

Freddie D. Spates, William D. Ledbetter, Sherman D. Minnigan, John W. Thompson, Kindra I. Carter, and Phillip D. Elliott

US Air Force
28th Operational Weather Squadron
Shaw Air Force Base, SC 29152

Final Report

Prepared for Headquarters, US Army Corps of Engineers
Washington, DC 20314-1000

Under PE 0603734A, Project T15

Abstract

Dust storms can be hazardous for aviation, military activities, and respiratory health and can occur on a wide variety of spatiotemporal scales with little to no warning. To properly forecast these storms, a comprehensive understanding of the meteorological dynamics that control their evolution is a prerequisite. To that end, we chose a major dust storm that occurred in Southwest Asia during July–August 2018 and conducted an observation-based analysis of the meteorological conditions that influenced the storm's evolution. We found that the main impetus behind the dust storm was a large-scale meteorological system (i.e., a cyclone) that affected Southwest Asia. It seems that cascading effects from this system produced a smaller, near-surface warm anomaly in Mesopotamia that may have triggered the dust storm, guided its trajectory over the Arabian Peninsula, and potentially catalyzed the development of a small low-pressure system over the southeastern end of the peninsula. This low-pressure system may have contributed to some convective activity over the same region. This type of analysis may provide important information about large-scale meteorological forcings for not only this particular dust storm but also for future dust storms in Southwest Asia and other regions of the world.

Contents

Figures and Tables

Figures

Tables

Preface

This study was conducted for Headquarters, US Army Corps of Engineers, under PE 0603734A, Project T15.

The work was performed by the Signature Physics Branch (Mr. Nathan Lamie, acting chief) and the Terrestrial and Cryospheric Sciences Branch (Dr. John Weatherly, chief) of the Research and Engineering Division, US Army Engineer Research and Development Center (ERDC), Cold Regions Research and Engineering Laboratory (CRREL). At the time of publication, Dr. Caitlin A. Callaghan was division chief. The acting deputy director of ERDC-CRREL was Mr. Bryan E. Baker, and the director was Dr. Joseph L. Corriveau.

The work was also performed by the Information Generation and Management Branch of the Geospatial Research Division, ERDC Geospatial Research Laboratory (GRL). At the time of publication, Mr. Michael F. Mailloux was branch chief, and Mr. Jeffrey B. Murphy was division chief. The deputy director was Ms. Valerie L. Carney, and the director was Mr. David R. Hibner.

The authors would like to thank Dr. Theodore Letcher at ERDC-CRREL, Mr. John Eylander at the ERDC Coastal and Hydraulics Laboratory, and Dr. Melissa Brooks at the United Kingdom Meteorological Office for their various contributions to this report.

This report contains modified Copernicus Climate Change Service Information (ECMWF 2012, 2019). The European Commission nor ECMWF (the European Centre for Medium-Range Weather Forecasts) is responsible for any use that may be made of the Copernicus information or data it contains.

COL Christian Patterson was commander of ERDC, and Dr. David W. Pittman was the director.

This page intentionally left blank.

1 Introduction

1.1 Background

Airborne dust, especially within dust storms, can be hazardous for aviation (Federal Aviation Administration 2020), military activities (McDonald et al. 2016), and respiratory health (Giannadaki et al. 2014). Additionally, dust storms are spatiotemporally diverse: they can form on any continent aside from Antarctica (Sissakian et al. 2013), propagate up to thousands of kilometers, and last from minutes (Arizona Emergency Information Network 2019) to days, potentially striking an area with little or no warning (Maricopa County 2021). However, proper forecasts of dust storms reduce their inherent risks. To that end, several numerical weather prediction models have incorporated dust-emission and transport schemes that allow forecasting of dust storms in various parts of the world (Liu et al. 2007; Johnson et al. 2011; Kok, Albani, et al. 2014; Kok, Mahowald, et al. 2014b; Terradellas et al. 2015; LeGrand et al. 2019; Ma et al. 2019). To develop these dust schemes and create high-quality dust-storm forecasts, it is important to have a comprehensive understanding of the dynamics of dust storms and the meteorological conditions that guide their evolution over space and time. Therefore, we selected a historical major dust storm from Southwest Asia as a case study for better understanding the relevant meteorological forcings that influence dust-storm development—from preconditions to initiation to cessation.

The dust storm in Southwest Asia selected for our case study had a large spatiotemporal footprint: from start to finish, it propagated about 2,000 km* from Iraq to the southernmost end of the Arabian Peninsula and affected the region for about 9 days (26 July to 3 August 2018). Furthermore, over the course of this event, dust was recorded in surface weather observations for at least four cities with more than one million inhabitants: Baghdad in Iraq, Riyadh in Saudi Arabia, and Abu Dhabi and Dubai in the United Arab Emirates (Weather Underground 2020). The dust storm was particularly persistent at Dubai International Airport, which reported "widespread dust" for 55 consecutive hours (Weather

* For a full list of the spelled-out forms of the units of measure used in this document and their conversions, please refer to *US Government Publishing Office Style Manual*, 31st ed. (Washington, DC: US Government Publishing Office, 2016), 245–252 and 345–347, https://www.govinfo.gov/content/pkg/GPO-STYLEMANUAL-2016/pdf/GPO-STYLEMANUAL-2016.pdf.

Underground 2020). Finally, the large spatiotemporal footprint of this dust storm allowed for a broader domain over which meteorological data could be gathered and analyzed.

The analyses of this study are important precursors for guiding future numerical simulations of this dust storm within Southwest Asia. In particular, while Francis et al. (2021) explored potential small-scale meteorological forcings of this dust storm over the Arabian Peninsula, our study also examines potential *large-scale* meteorological forcings farther upstream that may ultimately have predictive potential for the initiation of future dust storms. We expect that the combination of large-scale analyses (this study), small-scale analyses (this study and Francis et al. 2021), and future numerical simulations will ultimately lead to better understanding and prediction of the development of major dust storms not only in Southwest Asia but also worldwide.

1.2 Objective

The primary objective of this study was to identify the meteorological influences of the major dust storm that occurred in Southwest Asia in July–August 2018.

1.3 Approach

The first step of this study was identifying an appropriate geographical domain over which we would analyze meteorological data. Next, we obtained meteorological data from a variety of observation-based sources—surface-based stations, satellite products, atmospheric reanalyses, radiosondes, and precipitation products. We then used these data to conduct a quantitative and qualitative investigation of the meteorological environment surrounding the dust storm, including the creation of spatial maps and vertical cross sections of observation-based products and Skew-T plots of radiosonde data. Finally, we used the results of these analyses to formulate conclusions and recommendations that could inform future dust-storm analyses, both observational and model based.

2 Data and Methods

2.1 Study area

For the purposes of this report, Southwest Asia includes all countries bounded by the Mediterranean and Red Seas to the west; the Black and Caspian Seas to the north; the Persian Gulf, Gulf of Oman, and Arabian Sea to the east; and the Gulf of Aden and Arabian Sea to the south (Figure 1). This includes the entire Arabian Peninsula (Saudi Arabia, Kuwait, Bahrain, Qatar, the United Arab Emirates, Oman, and Yemen) and Mesopotamia (Iraq, Syria, and southeastern Turkey). Major topographic features of Southwest Asia include a stretch of higher elevations extending from Turkey into Iran, low-lying areas across Mesopotamia and around the Persian Gulf, the Al-Hajar Mountains at the southeastern end of the Arabian Peninsula, and an area of higher elevations on the Arabian Peninsula bordering the Red Sea and Gulf of Aden. Though Southwest Asia is dominated by the Arabian Desert, it also contains several densely populated areas, including the four populous cities that were affected by the dust storm (Baghdad, Riyadh, Abu Dhabi, and Dubai; Figure 1).

Figure 1. A map of Southwest Asia (adapted from Google 2022). The *orange* shapes on the map indicate the four major cities affected by the July–August 2018 dust storm: Baghdad (*circle*), Riyadh (*star*), Abu Dhabi (*square*), and Dubai (*triangle*).

In Sections 4 and 5, Figures 8–19 and 22–23 cover a larger area that encompasses not only Southwest Asia but also its surroundings (between 0° and 60° N and –10° and 80° E). Analyzing data over this larger area allows for a more accurate characterization of the meteorological environment up to several days in advance of the initiation of the dust storm.

2.2 Data sources

This report uses a variety of observational data sources to describe the meteorological environment for the July–August 2018 dust storm in Southwest Asia.

2.2.1 Station data

To identify trends in observed weather conditions during the dust storm, this report uses data from an archive of surface-based weather stations at Weather Underground (Weather Underground 2020). Hourly observations of quantitative and qualitative weather conditions within this dataset allow for a ground truth analysis of dust and wind at the surface.

2.2.2 Satellite products

To identify lofted dust over the study area, this report uses satellite imagery from the Spinning Enhanced Visible and InfraRed Imager (SEVIRI) instrument aboard the Meteosat Second Generation spacecraft, which is operated by the European Organisation for the Exploitation of Meteorological Satellites (EUMETSAT, "SEVIRI," n.d.). SEVIRI provides satellite images of aerosol optical depth (AOD) over the study area every 15 minutes that are used to infer the intensity of the dust storm (this report uses hourly data; EUMETSAT, "0 Degree," n.d.). This report also utilizes a snapshot from a video of Meteosat false-color satellite imagery that uses the DUST RGB filter (EUMETSAT 2022), which identifies dust in the atmosphere as shades of pink, purple, and magenta.

2.2.3 Atmospheric reanalyses

This study also relies on data from atmospheric reanalysis products, which incorporate millions of observational data points into a data assimilation scheme and weather model to create a spatiotemporally continuous atmospheric dataset that is constrained by observations. Atmospheric reanalyses can be especially useful for providing data in Southwest Asia, where surface-based weather observations are scarce.

Specifically, this examination uses data from two atmospheric reanalysis products: European Centre for Medium-Range Weather Forecasts (ECMWF) Reanalysis Interim (ERA-Interim) and v5 (ERA5). ERA-Interim provides global data from January 1979 to August 2019 at 3-hourly intervals, with a spatial resolution of approximately 80 km and 60 vertical levels from the surface to the 0.1 hPa pressure level (Dee et al. 2011; ECMWF 2012, 2020b). Meanwhile, ERA5 provides global data from 1959 to near-real time at hourly intervals, with a spatial resolution of approximately 30 km and 137 vertical levels from the surface to a height of 80 km above ground level (ECMWF 2019, 2020a; Hersbach et al. 2020). While ERA5 is the more recent reanalysis product, this report uses only the surface-based variables from ERA5, since using the large 3D atmospheric variables from ERA5 would have taken more time and resources than were feasible for this study. Therefore, this report instead uses the 3D atmospheric variables from ERA-Interim.

2.2.4 Radiosonde data

To better assess the convective environment with which the dust storm interacts, this report uses radiosonde data from an archive at the University of Wyoming that includes data from stations around the world (University of Wyoming, n.d.). Our report analyzes radiosonde data from this archive for Abu Dhabi International Airport (OMAA) and uses website-generated Skew-T plots, which show vertical profiles of air temperature, dewpoint temperature, and wind at various pressure levels.

2.2.5 Precipitation data

Finally, this report uses data from two precipitation products: the Climate Prediction Center (CPC) Global Unified Gauge-Based Analysis of Daily Precipitation (NOAA PSL 2020) and an analysis of precipitation observations utilizing the Land Information System (LIS; John Eylander, personal communication; Kumar et al. 2006). The CPC dataset has daily temporal resolution and 0.5° × 0.5° spatial resolution, and the LIS dataset has 3-hourly temporal resolution and 0.09° (~10 km) spatial resolution. While the CPC dataset relies on precipitation gauges only, the LIS dataset uses both gauge- and satellite-based observations. Radar-based products usually have a finer spatial resolution than the aforementioned datasets, but these types of products were not as readily available in Southwest Asia. Conversely, both of the precipitation products mentioned above were readily available for our domain of interest.

2.3 Methods

We conducted a quantitative and qualitative investigation of surface-based and upper-air meteorological data, including spatial maps and vertical cross sections of observation-based products and Skew-T plots of radiosonde data, for the July–August 2018 dust storm.

3 Description of the Dust Storm

The evolution of the dust storm can be split into four major phases—which we have termed *sweep*, *spread*, *spin*, and *drift*—between its initiation and conclusion.

3.1 Dust-storm initiation

The initiation of the dust storm occurred at around 0600 UTC (0900 local time) on 26 July 2018, as evidenced by a small area of high AOD (values greater than 1.00) observed in southwestern Iraq (Figure 2).

Figure 2. Values of aerosol optical depth (AOD) at 0600 UTC on 26 July 2018.

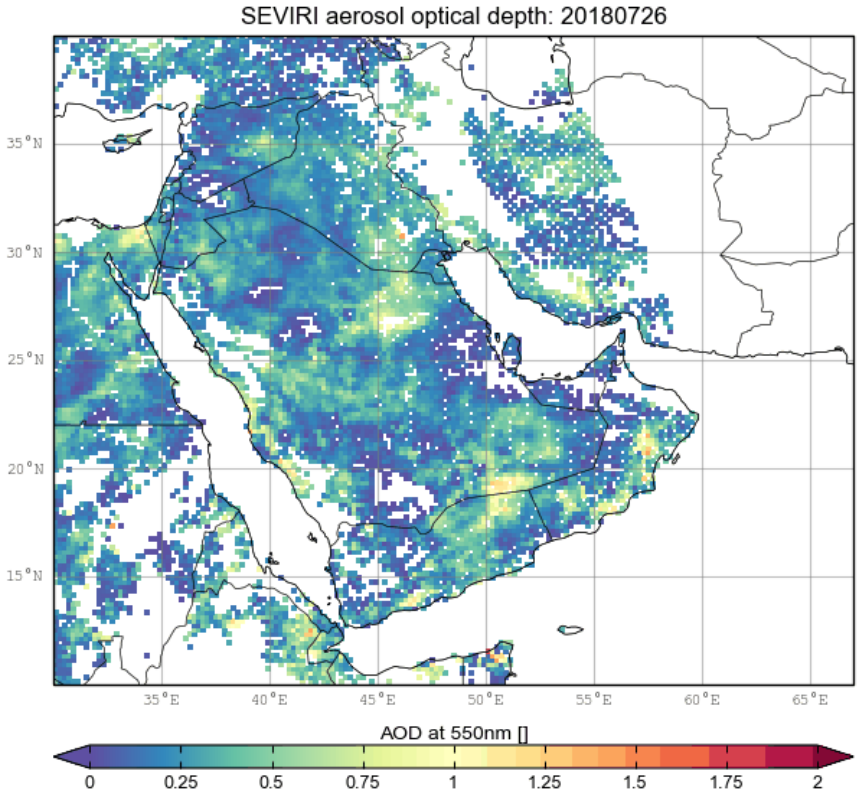

3.2 Sweep

For the next 24 hours, the cloud of dust greatly expanded in size (covering an area roughly equivalent to that of Syria) and became more intense (with widespread values of very high AOD [greater than 2.00]) as it "swept" to the south-southeast over the Arabian Peninsula (Figure 3). The propagation of the dust cloud was quite rapid: its leading edge traveled about

1,000 km between 0900 UTC on 26 July and 0830 UTC on 27 July (Google 2020), for an average speed of 42.6 km hr^{-1} (11.8 m s^{-1}).

Figure 3. Values of AOD at 1300 UTC on 26 July 2018.

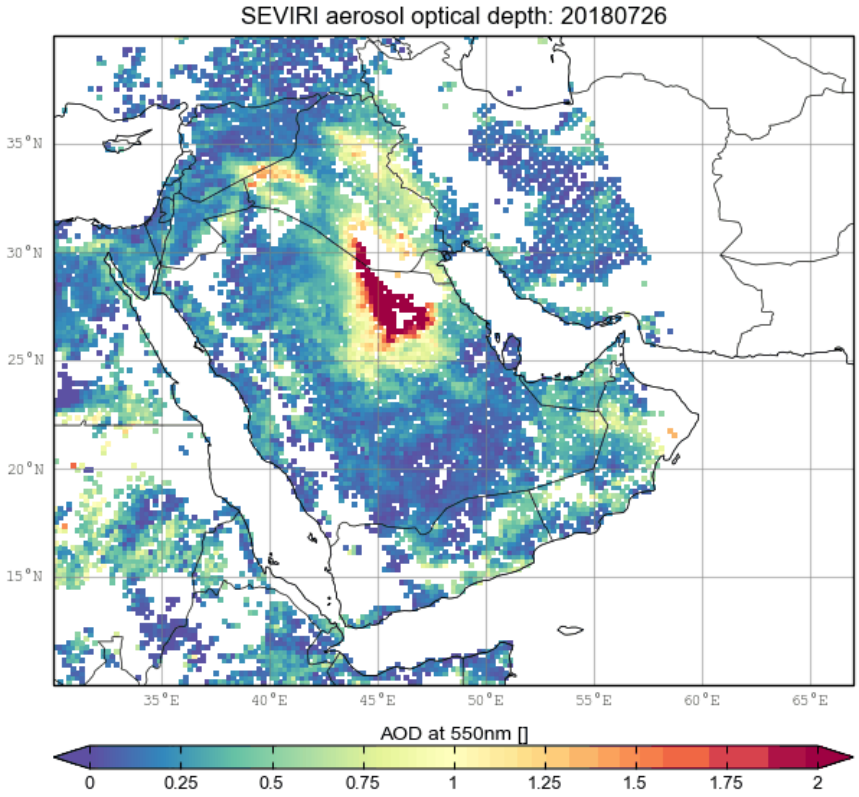

3.3 Spread

After sweeping across the Arabian Peninsula, the dust cloud began to "spread" zonally (west–east) beginning at about 0600 UTC on 27 July 2018 (Figure 4). While the western portion of the dust cloud propagated mostly off the southern end of the peninsula into the atmosphere over the Arabian Sea, the eastern portion slowed its propagation over the south-eastern end of the Arabian Peninsula until it came to a near standstill. According to EUMETSAT (Roesli 2018), this occurred because the dust cloud was blocked by the Al-Hajar Mountains in Oman and the United Arab Emirates (see Figure 1).

Figure 4. Values of AOD at 1000 UTC on 27 July 2018.

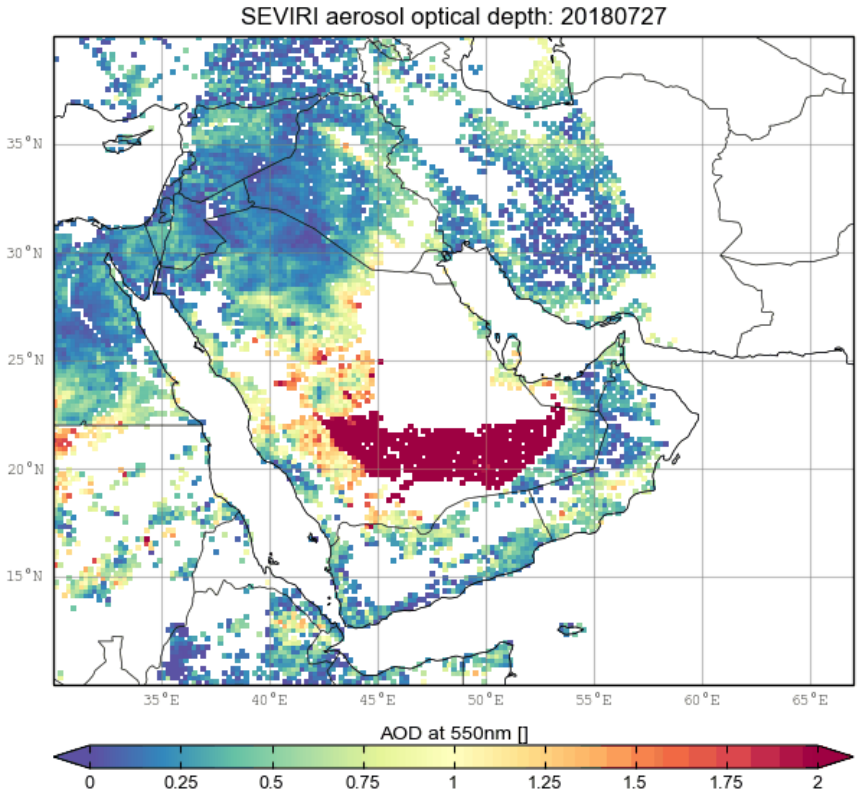

3.4 Spin

As the storm remained over the southeastern end of the Arabian Peninsula, the dust cloud began to "spin" counterclockwise, starting at around 2100 UTC on 28 July (Figure 5). The AOD values for the dust cloud remained high to very high for the duration of this phase.

3.5 Drift

After the spin phase, the dust cloud began to slowly "drift" to the southwest, beginning at about 1200 UTC on 30 July (Figure 6).

Figure 5. Values of AOD at 1800 UTC on 29 July 2018.

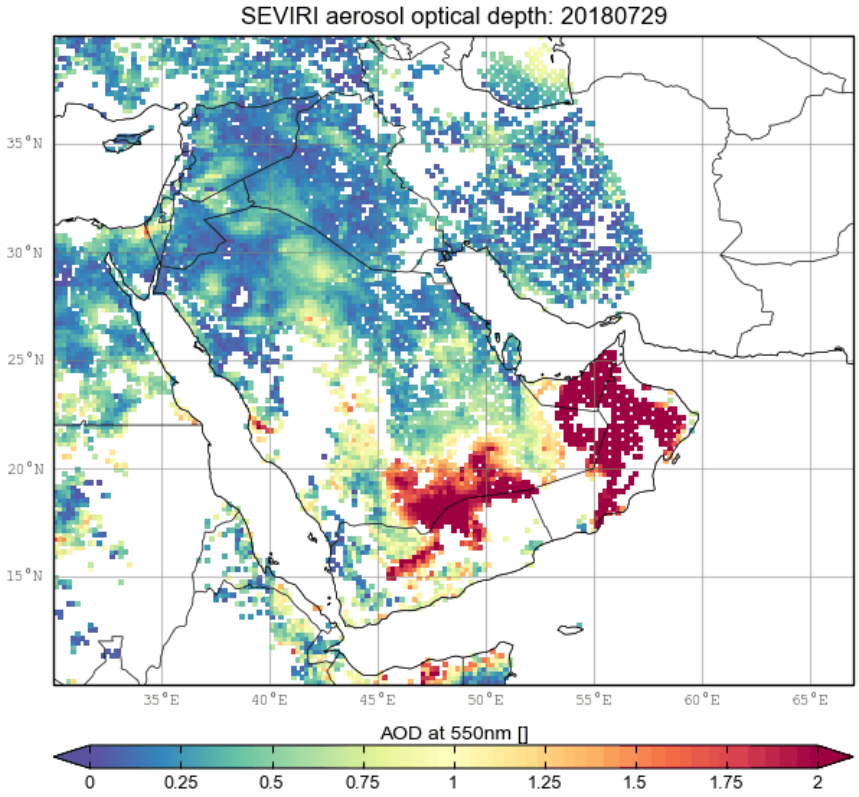

Figure 6. Values of AOD at 0600 UTC on 31 July 2018.

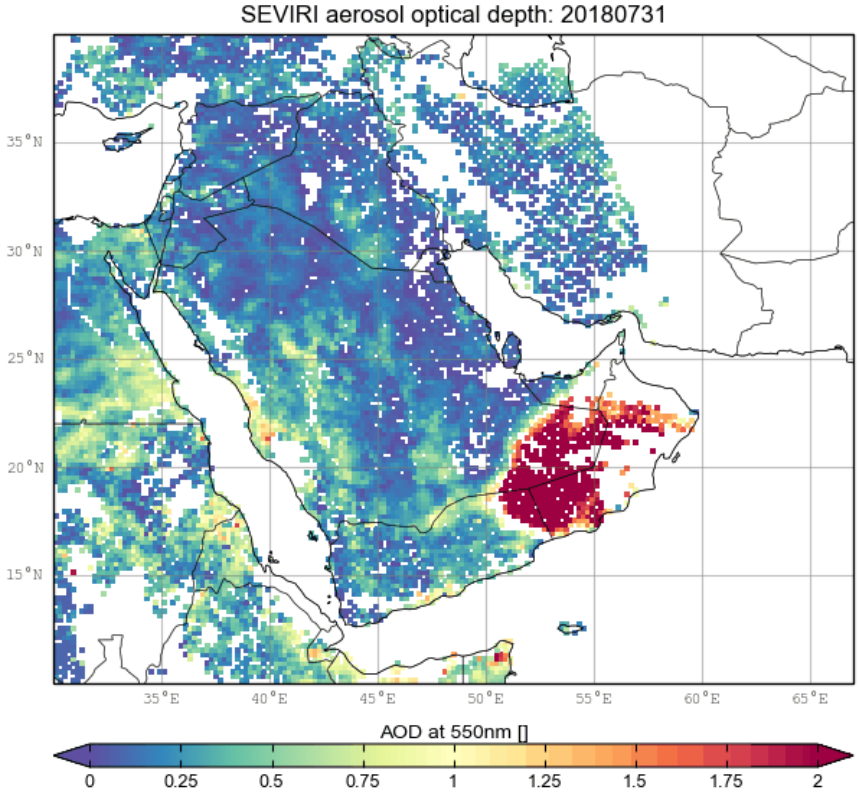

3.6 End of the dust storm

Finally, the last major areas of dust exited the Arabian Peninsula region by about 0600 UTC on 3 August (Figure 7).

Figure 7. Values of AOD at 0600 UTC on 3 August 2018.

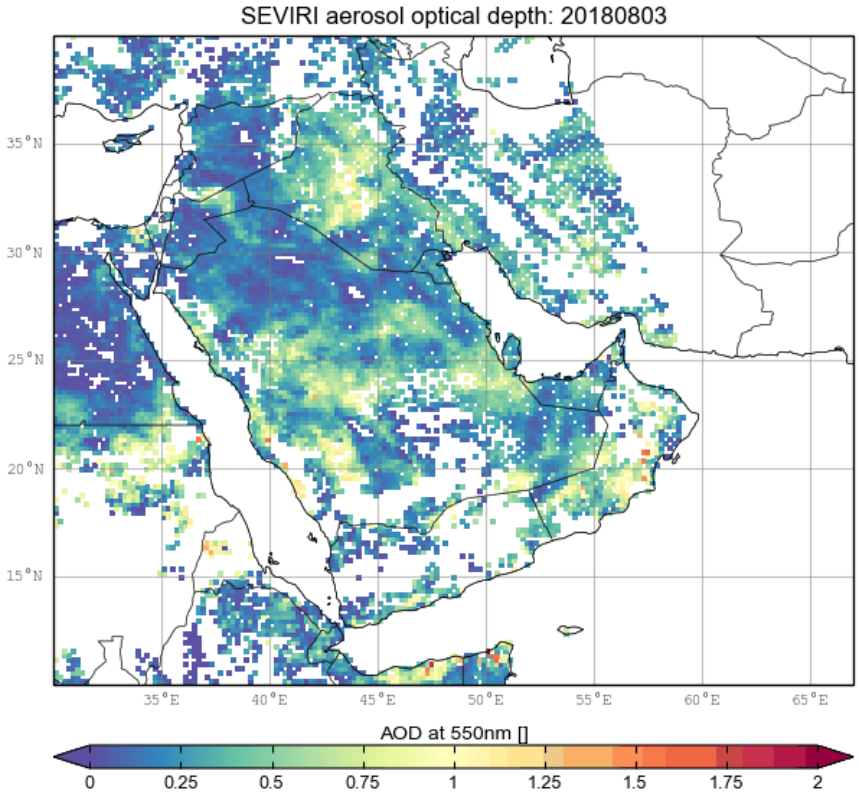

With this understanding of the general evolution of the dust storm, the following sections describe the meteorological conditions that preceded and coincided with this event and discuss the factors hypothesized to have contributed to its evolution.

4 Synoptic-Scale Meteorological Analyses

4.1 Timeline of events

Table 1 provides a timeline of (1) relevant atmospheric "milestones" that precede the initiation of the dust storm in Southwest Asia on 26 July and (2) the phases of evolution for the dust storm after its initiation. The table also includes the section numbers of this report that correspond with each milestone or phase and identifies whether there was dust in the surface-based observations for each of the four cities mentioned earlier in this report (along with the observed maximum sustained wind during the dust conditions). All of the surface weather observations in Table 1 were retrieved from Weather Underground (Weather Underground 2020).

Table 1. A timeline of atmospheric "milestones" that precede the initiation of the dust storm (up to and including 26 July 2018) and the phases of evolution for the dust storm after its initiation (26 July 2018 and later). For the four cities in the rightmost columns, cells are *orange* if the surface observations for any particular day indicate consecutive hours of dust that seem to be associated with the July–August 2018 dust storm (determined subjectively via satellite imagery). For these days, the number in each cell represents the maximum sustained wind (in miles per hour) at that station during times at which dust was reported (usually hourly; Weather Underground 2020).

Date (2018)	Milestone/Phase	Section	Observations of Wind Speed (mph) and Dust			
			Baghdad	Riyadh	Abu Dhabi	Dubai
18 Jul	"Control" conditions	4.2.1.1				
19 Jul						
20 Jul						
21 Jul	Trough appears	4.2.1.2				
22 Jul						
23 Jul	Jet streak emerges	4.2.1.3				
24 Jul	Trough deepens	4.2.1.4				
25 Jul	Arrival at Southwest Asia	4.2.1.5				
26 Jul	Initiation of dust storm / Sweep	4.2.1.6 / 4.2.2.1	31	17		
27 Jul	Spread	4.2.2.2		29		
28 Jul	Spin	4.2.2.3		25	14	
29 Jul				7	14	14
30 Jul	Drift	4.2.2.4			18	17
31 Jul					13	15
01 Aug						
02 Aug						
03 Aug	End of dust storm	4.2.3				

4.2 Spatial maps

4.2.1 Preceding the dust storm

4.2.1.1 "Control" conditions

The following subsections describe the *synoptic-scale* meteorological environment over Southwest Asia (i.e., meteorological features with length scales greater than 2,000 km). About 8 days prior to the dust storm, the synoptic-scale meteorological environment over Southwest Asia was characterized by generally seasonable atmospheric conditions—high air temperature at the 850 hPa pressure level, low humidity at the 700 hPa pressure level, and relatively low mean sea-level pressure (MSLP)—in a broad area surrounding the Persian Gulf (Figure 8). Additionally, moderately strong westerly to northwesterly winds (i.e., from the west to northwest) were present over Mesopotamia and the Persian Gulf from the surface up to the 700 hPa pressure level, which bears similarity to the summertime shamal (strong, low-level northwesterly winds; Yu et al. 2016).

Above the surface, it can be useful to analyze patterns in other meteorological variables as well. For example, geopotential (GP, "the potential energy of a unit mass relative to sea level" [American Meteorological Society 2017]) and its derivative—geopotential height—can be used to locate troughs and ridges at various atmospheric-pressure levels. Lower levels of GP are indicative of lower mean temperatures between the surface and the chosen pressure level. The geopotential height usually decreases from south to north in the northern hemisphere, reflecting the latitudinal variation of mean temperature within the troposphere (the lowest layer of the atmosphere). Regions where relatively low GP dips south are called *troughs* and are often associated with cyclonic wind flow and unsettled weather in the midlatitudes. On the other hand, higher levels of GP that bulge northward are called *ridges* and are often associated with broad regions of sinking air in the troposphere and quiescent weather at the surface.

At the 500 hPa pressure level, a prominent area of higher GP was situated over northwestern Africa (with a ridge to the north of it), and an elongated area of lower GP was present over eastern Europe (with a trough to the south of it). Higher in the atmosphere, relatively zonal flow (no large south–north fluctuations) and generally westerly winds were evident at 200 hPa.

Figure 8. "Control" atmospheric conditions over Southwest Asia and its surroundings at 0000 UTC on 18 July 2018, 8 days before the initiation of the dust storm. *Left column,* various atmospheric variables. *Top to bottom*: Mean sea-level pressure (MSLP), air temperature at the 850 hPa pressure level, relative humidity at the 700 hPa pressure level, and geopotential (GP) at the 500 hPa pressure level. *Right column*, wind speed at various vertical levels. *Top to bottom*: the surface (10 m above ground level), 850 hPa, 700 hPa, and 200 hPa.

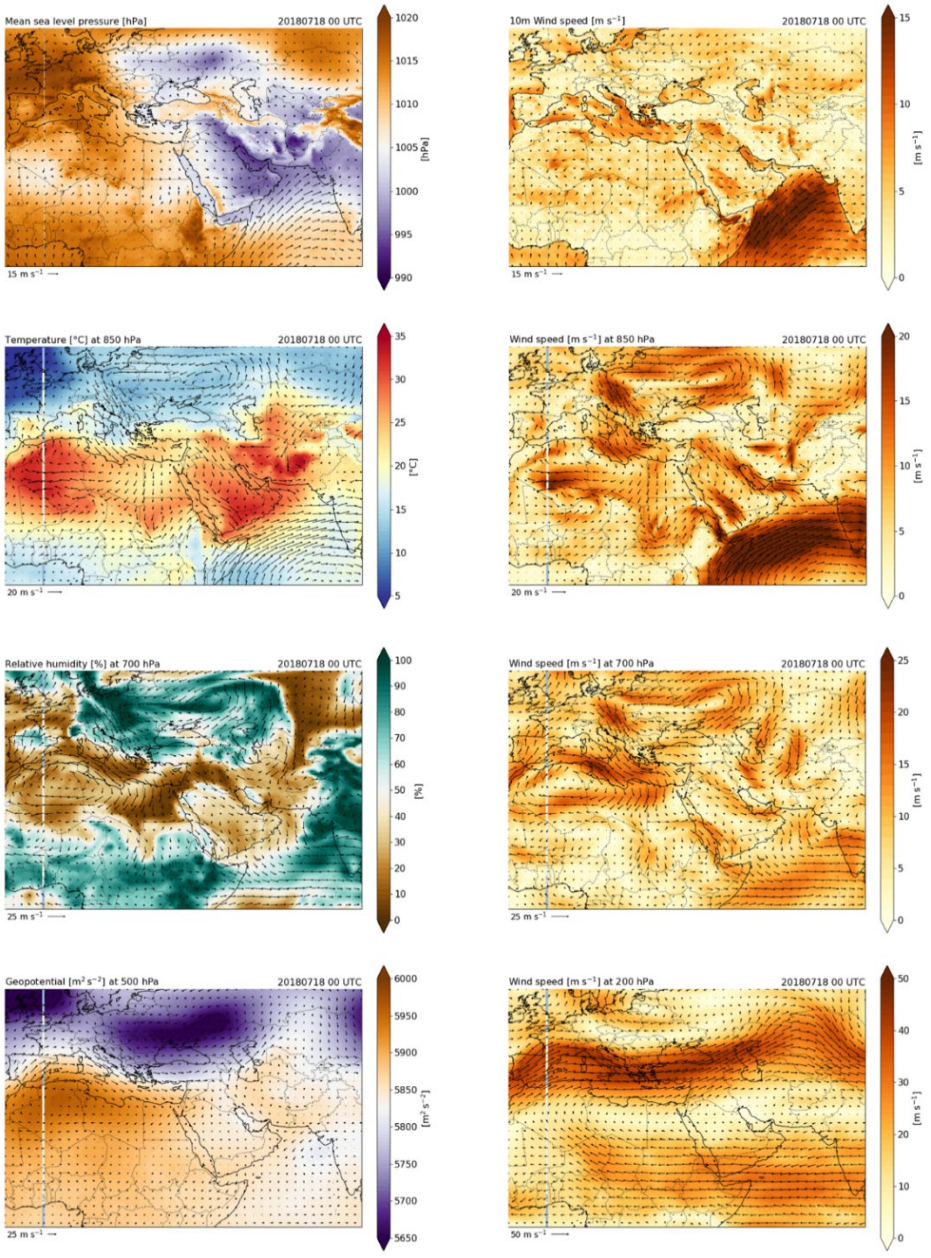

4.2.1.2 Trough appears

At about 1200 UTC on 21 July, the meteorological situation began to change: an upper-air trough entered western Europe, which is visible in the wind field for 200 hPa and in an area of lower GP at 500 hPa (Figure 9).

Figure 9. Atmospheric conditions over Southwest Asia and its surroundings at 1200 UTC on 21 July 2018. (This figure and Fig. 10–16, 18, and 19 have similar figure layouts and caption information to Fig. 8.)

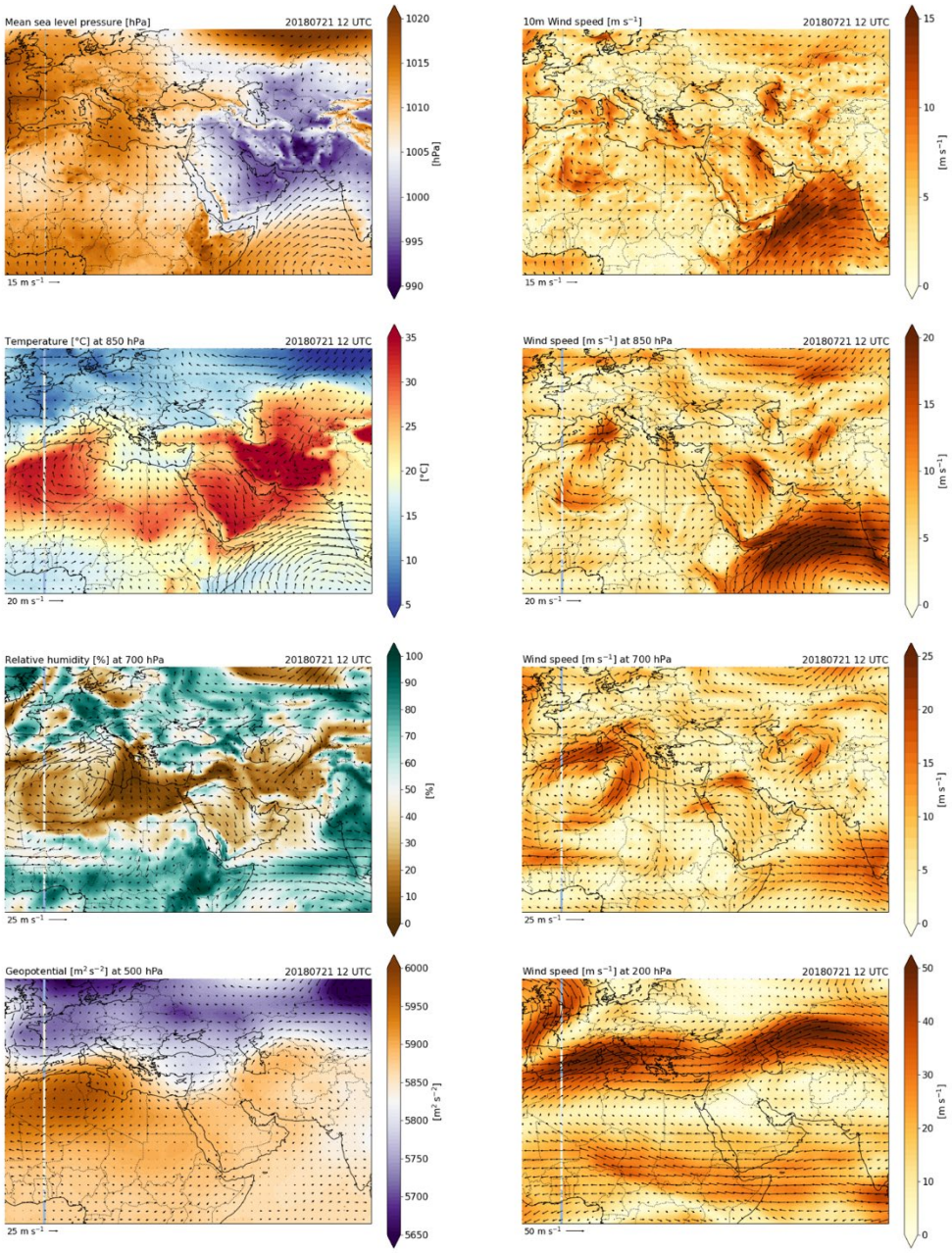

4.2.1.3 Jet streak emerges

As the trough propagated eastward, its associated area of lower GP at 500 hPa edged closer to the aforementioned area of lower GP over eastern Europe (Figure 10). Simultaneously, a ribbon of higher wind speeds became evident at 850 and 700 hPa over the Mediterranean Sea at around 0000 UTC on 23 July. This ribbon of higher wind speeds is associated

with a broader ribbon of strong winds in the upper troposphere (200 hPa) that is referred to as the *jet stream*. The local peak of higher winds at lower levels may therefore be considered to be a low-level jet *streak*. Jet streaks are often precursors to *cyclogenesis* (cyclone development) at midlatitudes; and as the following subsections illustrate, the appearance of this jet streak portends the development of a cyclone within this domain.

Figure 10. Atmospheric conditions over Southwest Asia and its surroundings at 0000 UTC on 23 July 2018. The *white X*'s in the *bottom-left* panel of this figure and the next two figures denote minima of GP that merge over time.

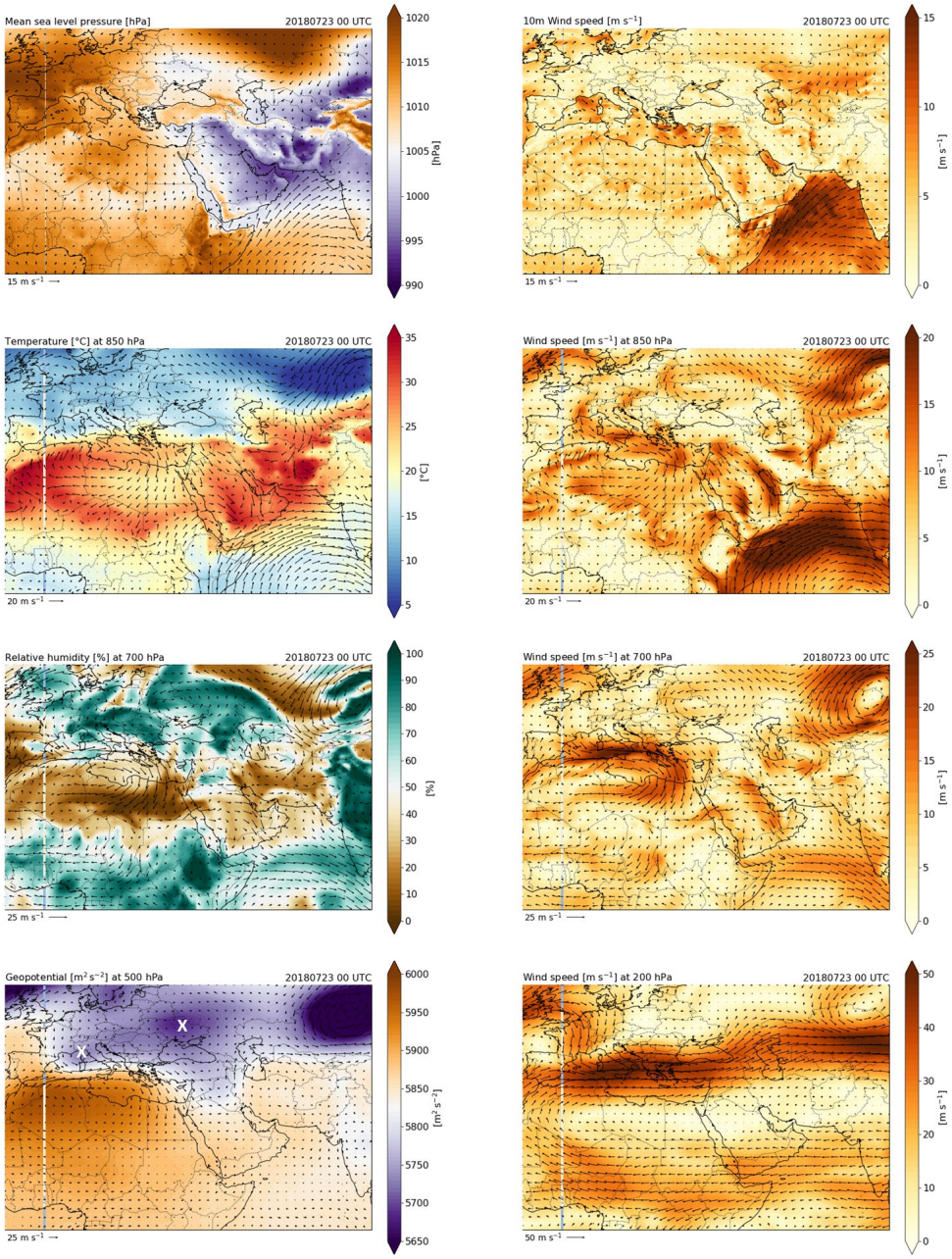

4.2.1.4 Trough deepens

A day later (at 0000 UTC on 24 July), the trough had deepened and tilted in a slightly less positive direction, which is evident in the 200 hPa wind field (Figure 11). The two previously distinct areas of lower GP at 500 hPa also began to merge. As this process unfolded, the jet streak over the Mediterranean Sea extended upstream into eastern Europe and increased in magnitude at 850 hPa. Furthermore, the jet streak extended downward toward the surface, manifesting as a coherent area of stronger surface winds over the central Mediterranean Sea.

4.2.1.5 Arrival at Southwest Asia

By 0000 UTC on 25 July, the two previously distinct areas of lower GP at 500 hPa had merged, and the trough at 200 hPa had switched from a positive to a negative tilt, indicating maturity of the associated weather system (Figure 12). Indeed, at 700 hPa, winds were rotating in a counterclockwise fashion in the same region, which likely indicates that a mature cyclone had formed. At this time, the jet streak had arrived at the eastern end of the Mediterranean Sea, about to enter Southwest Asia. Additionally, a region of colder air at 850 hPa emerged just to the west of the area of lower GP, and a ribbon of drier air at 700 hPa became evident near the area of stronger winds over the Mediterranean Sea.

4.2.1.6 Dust-storm initiation

However, around the time of the initiation of the dust storm (0600 UTC on 26 July), an interesting meteorological development occurred: a ridge at 200 hPa slightly amplified and shifted westward over the Caspian Sea (Figure 13). This is likely associated with an area of higher GP that developed in western Iran, blocking the eastward propagation of both the trough and the merged area of lower GP. Thus, the upper-tropospheric dynamics stalled out. However, several lower-tropospheric trends continued unabated: the jet streak at 850 and 700 hPa continued to propagate from the Mediterranean coast into Mesopotamia, colder air at 850 hPa continued to edge into the Syrian Desert, and a front of dry air at 700 hPa propagated into Iraq off the Mediterranean Sea. Finally, moderately strong winds emerged at the surface in a broad area from Iraq to the southern Arabian Peninsula.

Figure 11. Atmospheric conditions over Southwest Asia and its surroundings at 0000 UTC on 24 July 2018.

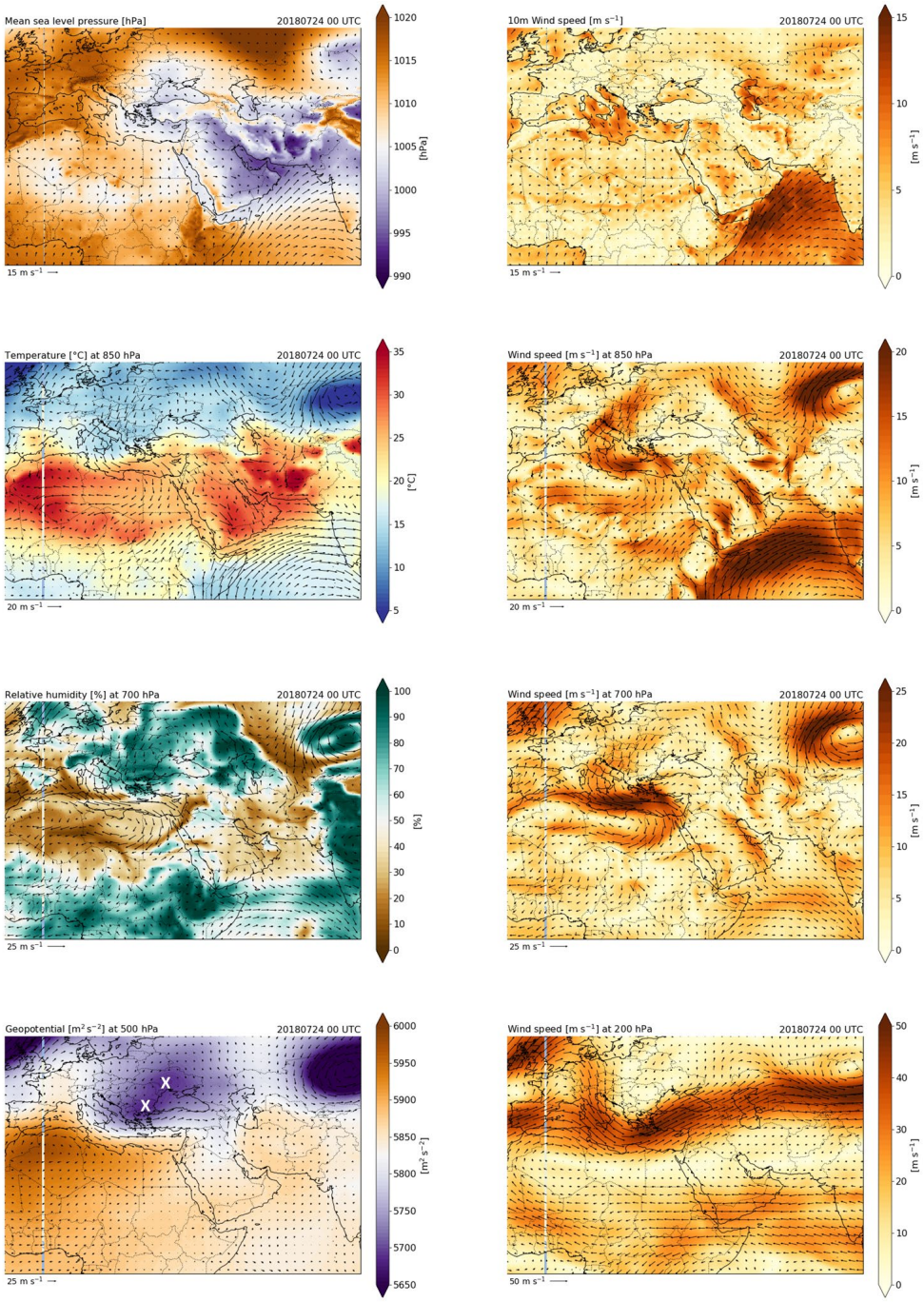

Figure 12. Atmospheric conditions over Southwest Asia and its surroundings at 0000 UTC on 25 July 2018.

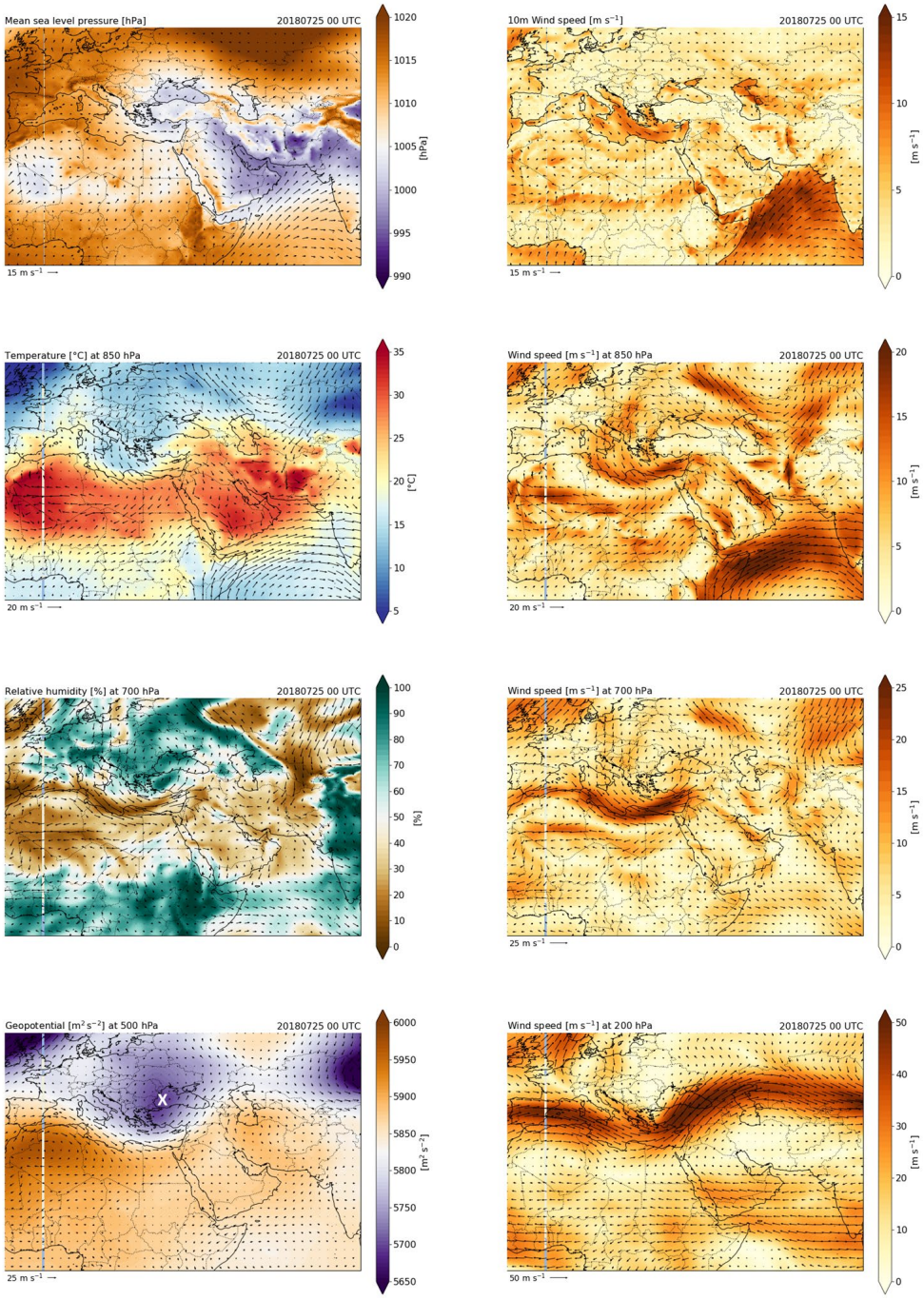

Figure 13. Atmospheric conditions over Southwest Asia and its surroundings at 0600 UTC on 26 July 2018.

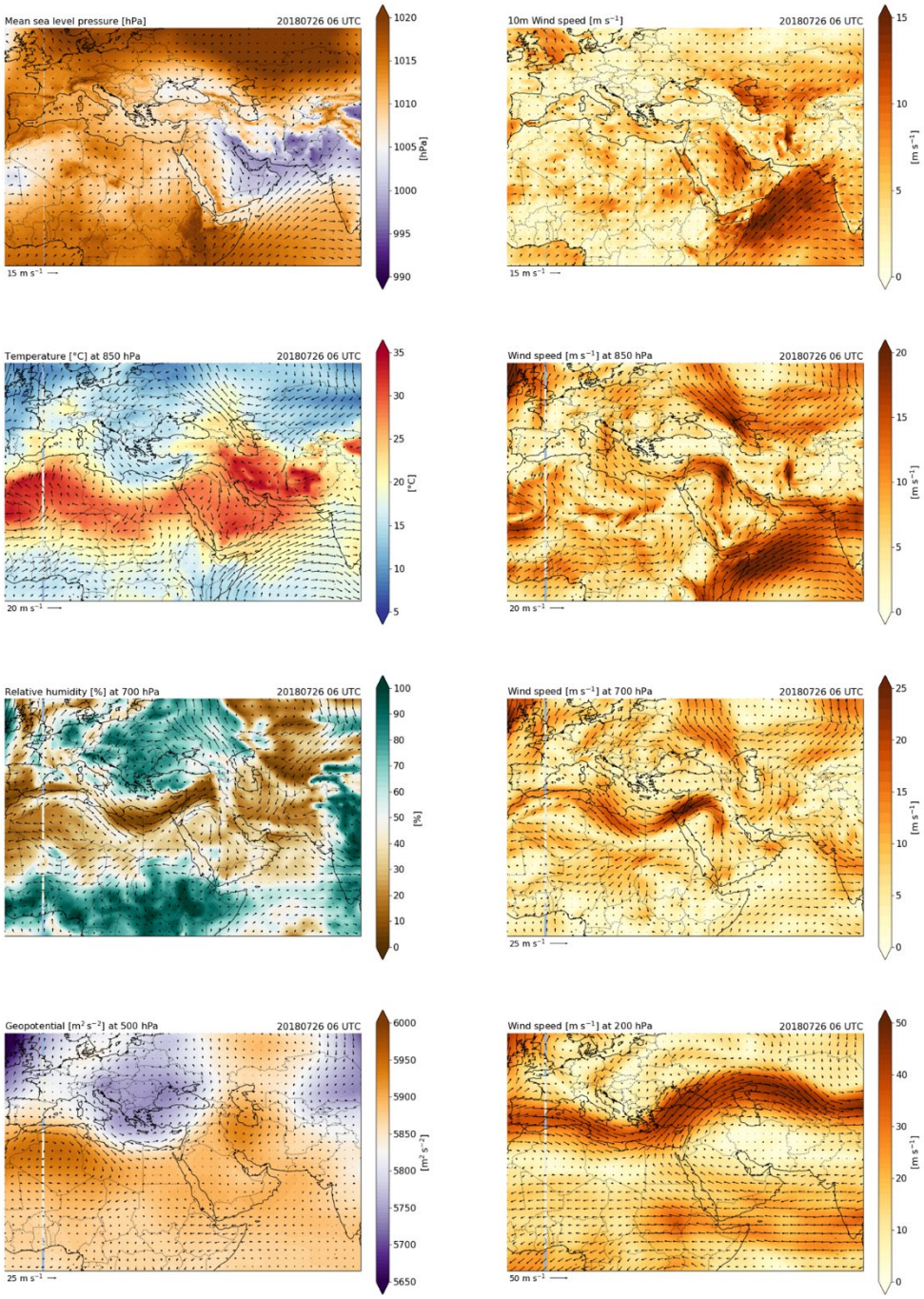

Interestingly, surface winds near the meeting point of Iraq, Kuwait, and Saudi Arabia (close to the origin of the dust storm) had actually peaked the day before the initiation of the dust storm (at 1200 UTC on 25 July; not shown). Therefore, one might wonder why the dust storm did not begin a day earlier. One potential reason for this is that after dust is lofted by surface winds, it likely requires strong winds higher in the atmosphere to transport it longer distances. Winds at 850 hPa over Mesopotamia were weaker on 25 July than on 26 July (see Figures 12 and 13); so even if dust had been lofted from the surface on 25 July, it may not have stayed aloft as long or propagated as far as it did on 26 July. There may have been other contributing factors as well, but elucidating them likely requires additional analyses beyond the scope of this study.

In summary, upper-tropospheric dynamics had seemed favorable for a well-developed cyclone to enter Southwest Asia shortly before the initiation of the dust storm. However, after an upper-tropospheric ridge blocked the eastward progression of the cyclone, it seems that the energy that it harbored may have propagated lower into the troposphere before continuing into Southwest Asia.

4.2.2 During the dust storm

4.2.2.1 Sweep

During the sweep phase, as the upper-tropospheric dynamics continued to stall, lower-tropospheric dynamics remained favorable for rapid dust propagation. For example, the jet streak at 850 hPa in Mesopotamia actually strengthened and extended southward into the Arabian Peninsula, and the area of moderately strong winds at the surface became narrower but retained its intensity (Figure 14). Additionally, MSLP began to decrease across the Persian Gulf, perhaps in response to some energy from the cyclone that propagated to the southeast of Iraq. Finally, moderately strong winds at 700 hPa pushed southward into the Arabian Peninsula, carrying drier air from both the Syrian Desert and Iran. The dry air aloft likely contributed to the lack of precipitation near the origin of the dust storm (see the precipitation analyses in Section 5.1).

Figure 14. Atmospheric conditions over Southwest Asia and its surroundings at 0600 UTC on 27 July 2018.

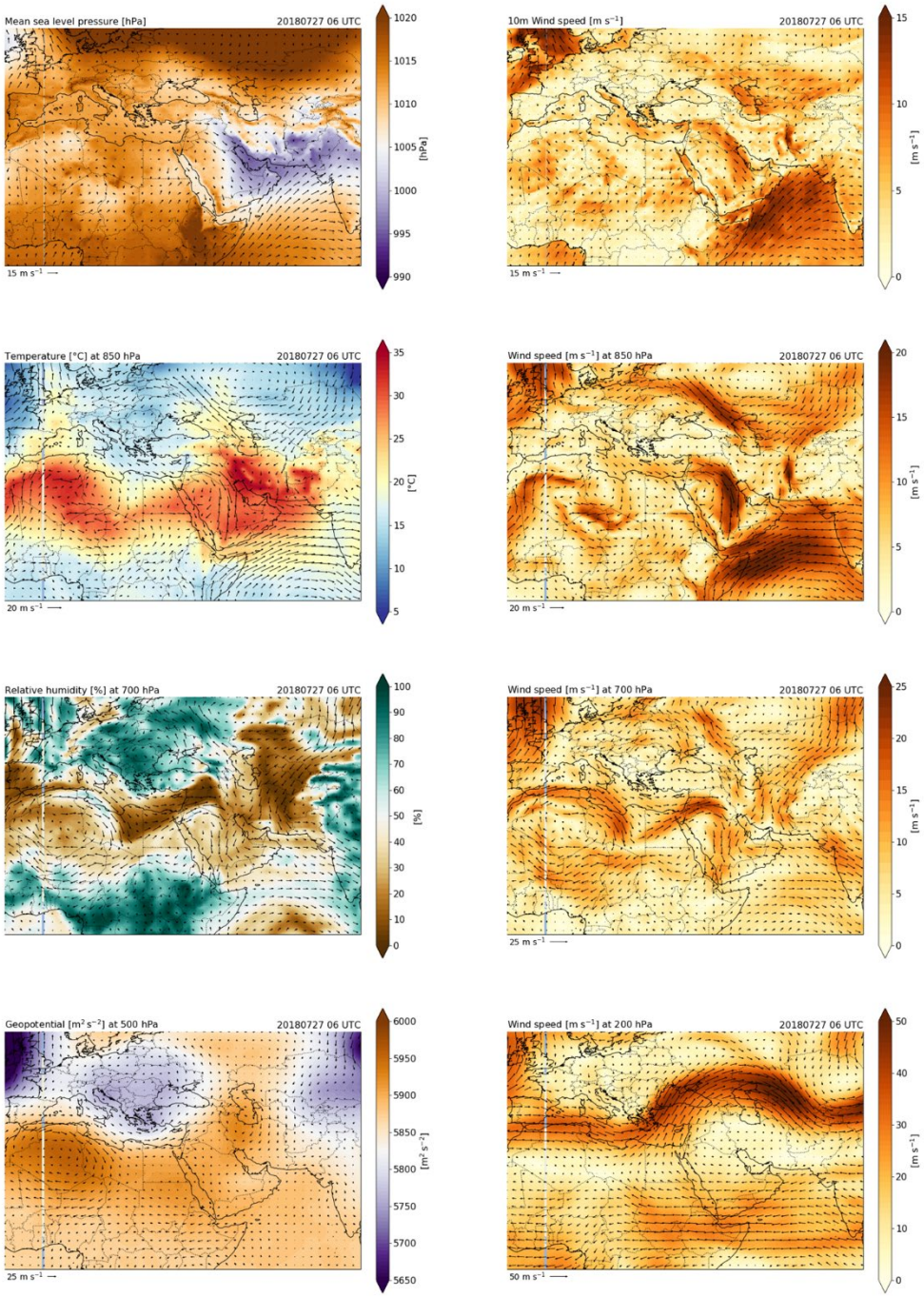

4.2.2.2 Spread

During the spread phase, westerly to northerly winds at 850 hPa remained strong over the northern portion of the Arabian Peninsula, but westerly winds over the southeastern portion of the Arabian Peninsula slightly strengthened (Figure 15). This is important because without the stronger

westerly winds, most (if not all) of the dust from the dust storm would have likely propagated off the southern end of the Arabian Peninsula into the Arabian Sea. The slight strengthening in westerly winds may have been influenced by the Somali Jet, a low-level jet originating near Somalia and blowing northeastward across the Arabian Sea. The combination of stronger westerly winds and the topography of the Al-Hajar Mountains (see Section 3.3) likely contributed to the dust cloud propagating toward and remaining over the southeastern end of the Arabian Peninsula.

Meanwhile, surface winds weakened over the Arabian Peninsula (likely due to diurnal cooling), and values of MSLP over the Persian Gulf continued to decrease (Figure 15). By this time, the stalled area of lower GP had also begun to weaken over eastern Europe.

4.2.2.3 Spin

During the spin phase, a small low-pressure area developed over the southeastern end of the Arabian Peninsula, which is evident in the map of MSLP (Figure 16). Additionally, some counterclockwise spin was present in wind fields at the surface and at 850 and 700 hPa. The dust cloud also followed this small-scale circulation pattern, wrapping around the area of lower pressure (see Figure 5). One source suggests that this low-pressure area was a *thermal low*, in which intense heating of the surface reduces the density of the air, causing upward vertical motion in the lower troposphere (Roesli 2018). Another source suggests that this low-pressure area formed as a result of radiative differences caused by the dust cloud over the Arabian Peninsula (Francis et al. 2021). Regardless of the cause, this low-pressure area may be evident as a slight warm anomaly at 850 hPa located over the southeastern end of the Arabian Peninsula (Figure 16).

An interesting meteorological development paralleled the formation of this low-pressure area. In maps of surface temperature at 0000 UTC, a weak warm anomaly developed over Mesopotamia on 26 July and propagated to the south-southeast across the Arabian Peninsula, closely following the dust cloud (Figure 17). By 29 July, this warm anomaly seemed to break apart, with one portion drifting to south-central Saudi Arabia and another portion propagating eastward to the southeastern quadrant of the Arabian Peninsula. By 30 July, two adjacent warm anomalies remained over the southeastern quadrant of the Arabian Peninsula in the vicinity of the low-pressure center.

Figure 15. Atmospheric conditions over Southwest Asia and its surroundings at 1800 UTC on 27 July 2018.

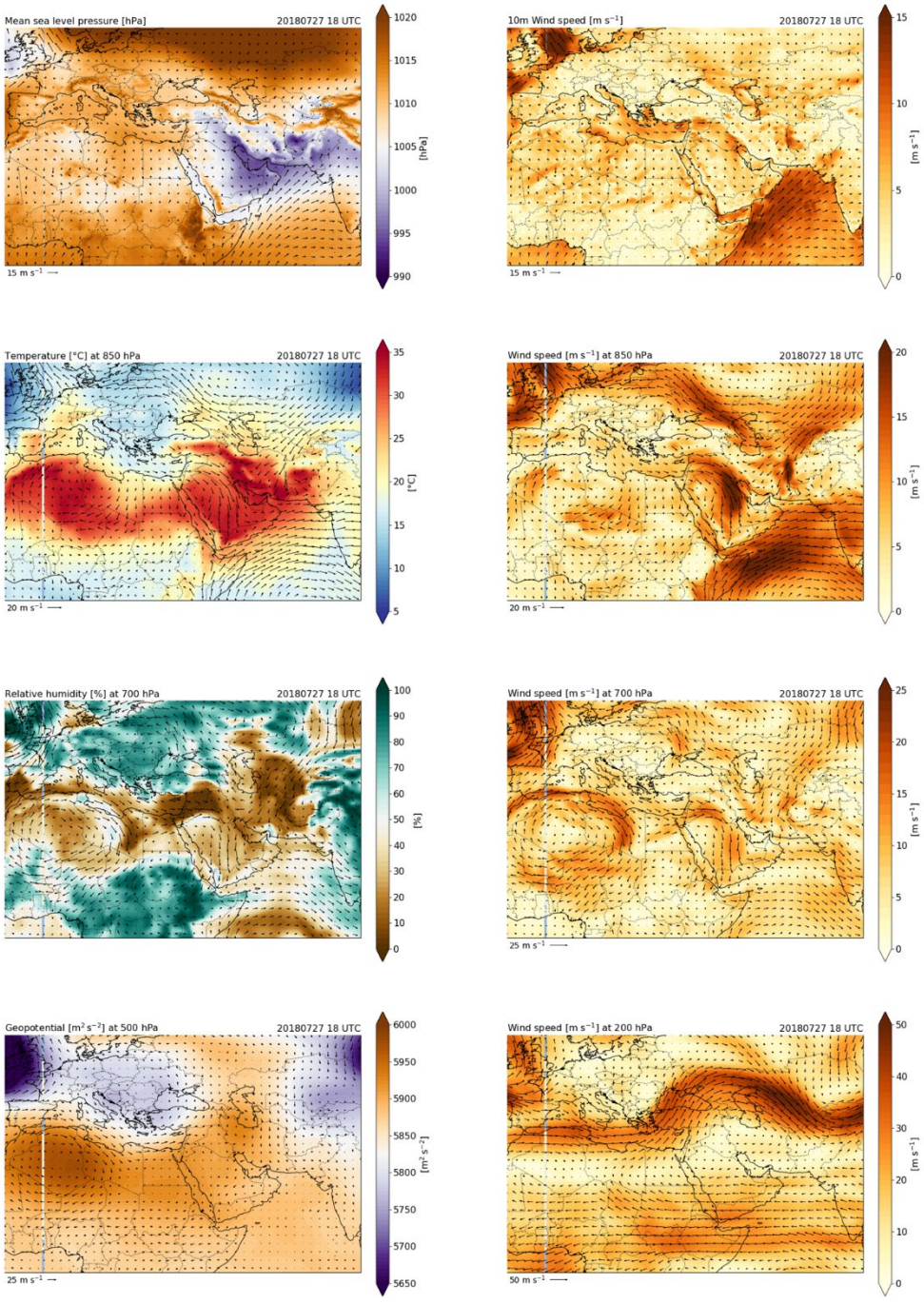

Figure 16. Atmospheric conditions over Southwest Asia and its surroundings at 1200 UTC on 29 July 2018. The *white X* in the *upper-left* panel of this figure denotes the small low-pressure area mentioned in the previous paragraph.

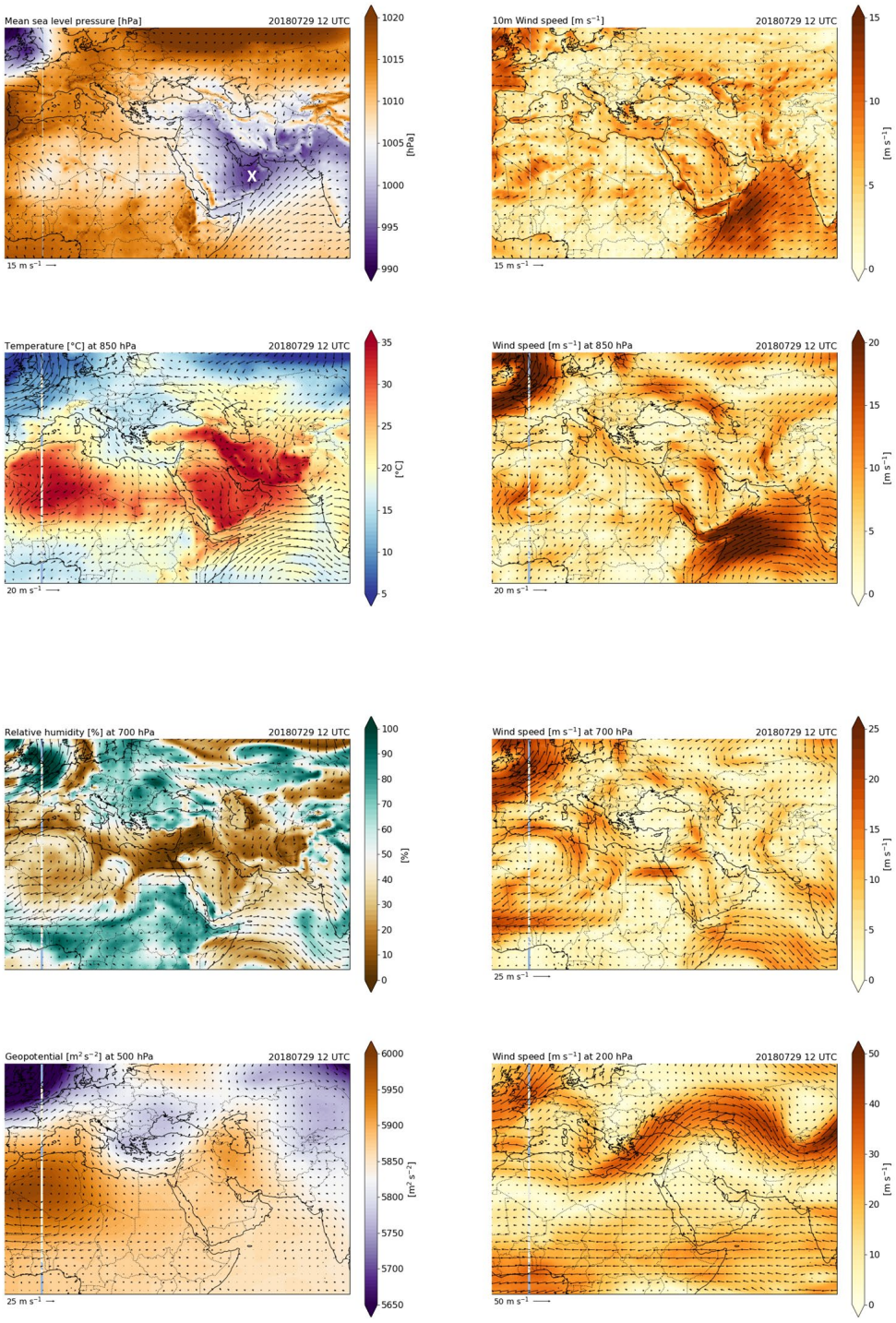

Figure 17. *Left*, air temperature at the surface (2 m above ground level, in degrees Celsius); *middle and right*, anomalies of air temperature at the surface and at 850 hPa, respectively. The anomalies are calculated with respect to the "control" conditions (0000 UTC on 18 July 2018). *Top to bottom*: Snapshots at 0000 UTC from 23 to 30 July. *Black arrows* in the *left* and *middle* columns show the locations of the warm anomalies discussed in the main text.

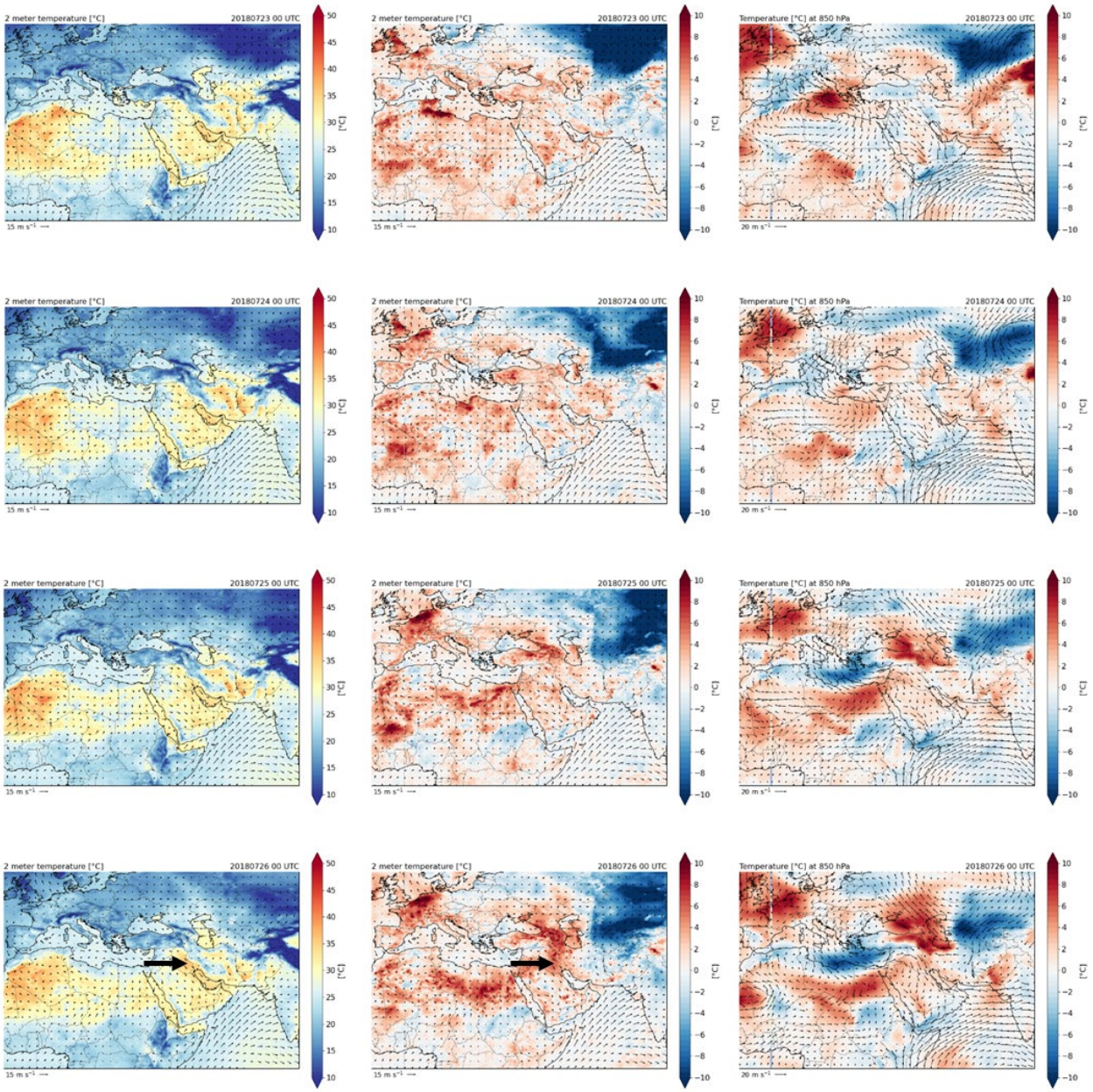

Figure 17 (cont.). *Left*, air temperature at the surface (2 m above ground level, in degrees Celsius); *middle and right*, anomalies of air temperature at the surface and at 850 hPa, respectively. The anomalies are calculated with respect to the "control" conditions (0000 UTC on 18 July 2018). *Top to bottom*: Snapshots at 0000 UTC from 23 to 30 July. *Black arrows* in the *left* and *middle* columns show the locations of the warm anomalies discussed in the main text.

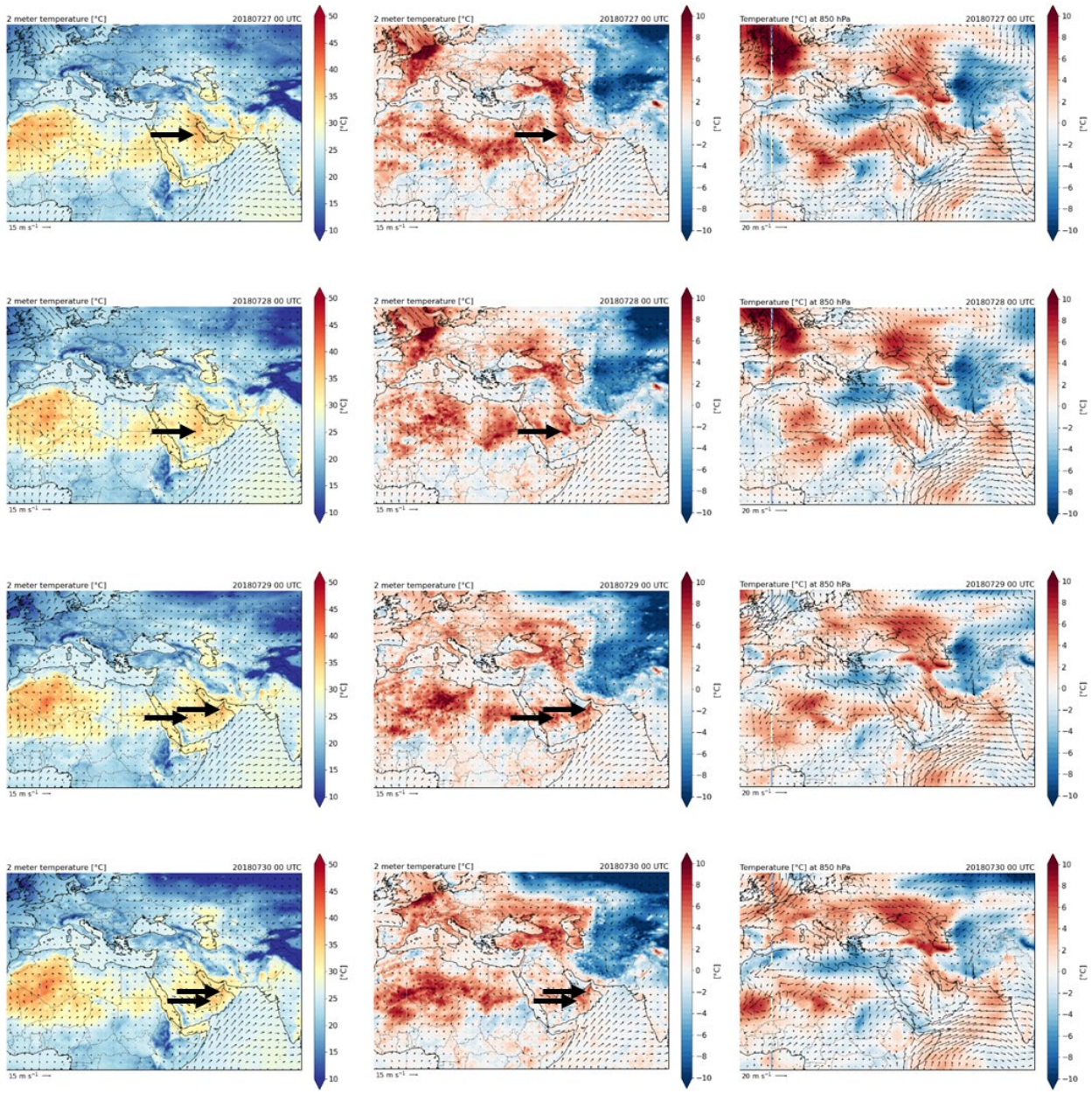

This warm anomaly seems to have been influenced by larger-scale meteorological mechanisms that preceded the initiation of the dust storm. In Figure 17, anomalies of air temperature at the surface and at 850 hPa show a "pulse" of warmer air traversing the Mediterranean Sea on 23 July (i.e., warm air advection). Two days later, on 25 July, this warm pulse had split into two pockets of warmer air at 850 hPa to the south and east-northeast of a cooler anomaly in the eastern Mediterranean Sea. By 26 July, just before the initiation of the dust storm, a sweeping arc of warm surface temperature anomalies had formed in the region, extending from eastern Algeria to the northern coast of the Black Sea, with the Mesopotamian warm anomaly located in the southeastern portion of the arc. Over the next several days, the arc of warm anomalies (and the Mesopotamian warm anomaly) expanded to the south-southeast over the Arabian Peninsula until reaching a "critical" latitude of about 20° N, at which the arc stopped its southward progression and slowly disintegrated. While this expanding arc of warm anomalies was not as evident at 850 hPa, warm anomalies still expanded over the Persian Gulf during a similar time frame.

The above evidence seems to indicate that the warm anomaly that propagated over the Arabian Peninsula originated with the synoptic-scale system that traversed the Mediterranean Sea. As the system injected energy into the lower troposphere over a broad arc in Southwest Asia and its surroundings, it seems to have generated the warm anomaly in Mesopotamia, which may have served as a trigger for the dust storm. This warm anomaly may have also guided the trajectory of the dust storm across Southwest Asia and, perhaps, the development of the aforementioned low-pressure area in the southeastern quadrant of the Arabian Peninsula.

4.2.2.4 Drift

The area of low pressure over the southeastern portion of the Arabian Peninsula weakened during the drift phase, and lower-tropospheric winds in the region became slightly stronger, shifting to a more northerly pattern at 850 and 700 hPa (Figure 18). Additionally, winds at 500 hPa shifted to a more northeasterly pattern. Especially in the absence of other major changes in the upper troposphere (the previous area of lower GP had almost completely eroded by this point), these shifts in wind likely guided the dust cloud slowly over the rest of the southern Arabian Peninsula until its exit into the Arabian Sea.

Figure 18. Atmospheric conditions over Southwest Asia and its surroundings at 1800 UTC on 31 July 2018.

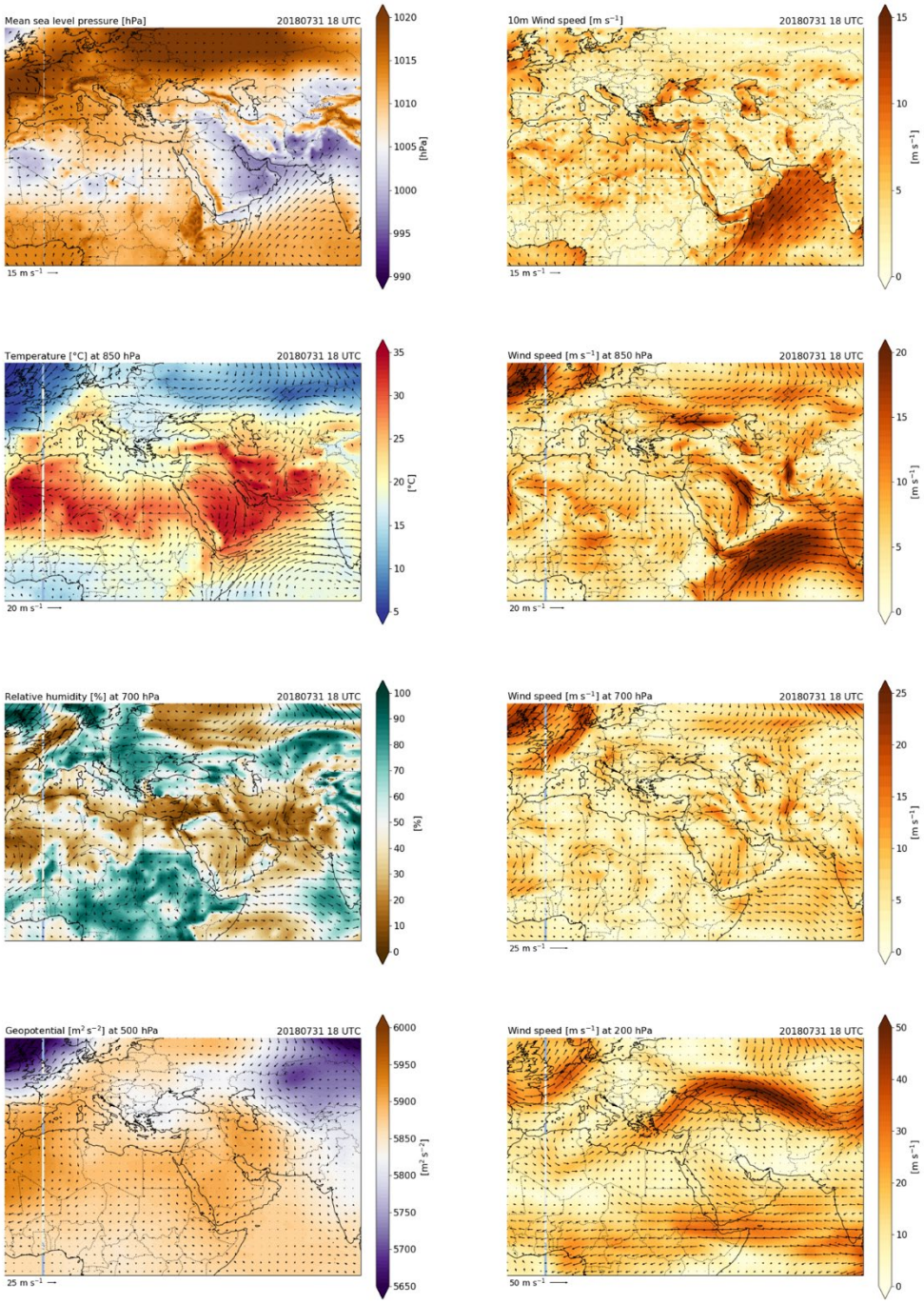

4.2.3 End of the dust storm

By about 0600 UTC on 3 August, the last major portions of dust exited the peninsula, and the atmosphere over Southwest Asia returned to a state similar to that of the "control" conditions 8 days before the dust storm (Figure 19).

Figure 19. Atmospheric conditions over Southwest Asia and its surroundings at 0000 UTC on 3 August 2018. The *horizontal* and *vertical black lines* in the *lower-left* panel are transects over which vertical cross sections are taken in Figs. 20 and 21, respectively.

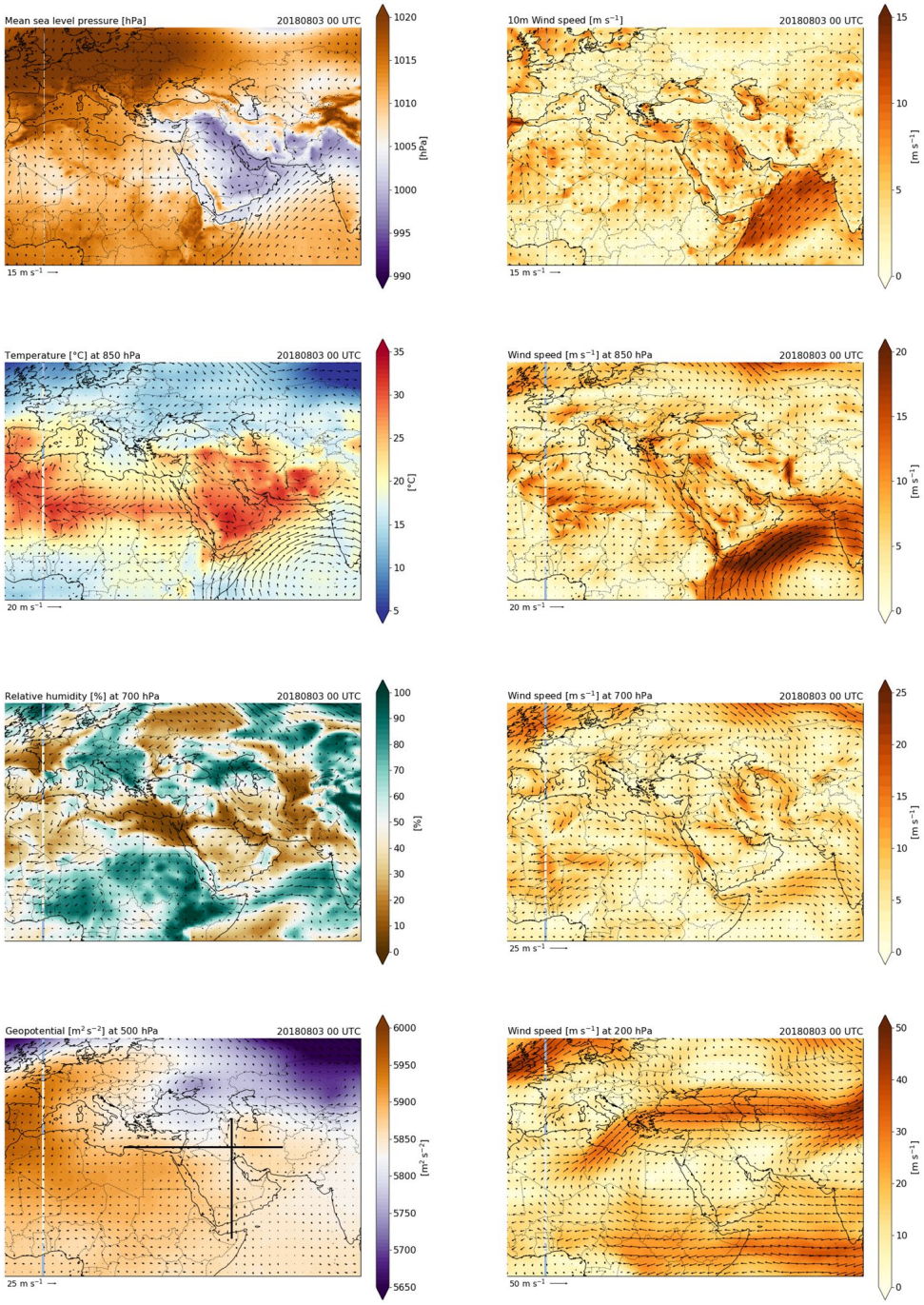

4.3 Vertical cross sections

While Figures 8–19 are helpful for illustrating the spatial patterns of several atmospheric variables across the geographic domain, they are generally limited to individual time steps and vertical levels. Therefore, to expand the temporal and vertical coverage of our analyses, we also created time-phased vertical cross sections of wind speed, temperature, and relative humidity (Figures 20 and 21). Similar to Figure 17, the vertical cross sections depict anomalies in atmospheric variables (relative to the "control" conditions at 0000 UTC on 18 July 2018) to better illustrate changes from the "control" pattern of the atmosphere at each location. Note that the plots in Figures 20 and 21 use data from ERA-Interim only; the surface values from ERA5 are not included.

Figure 20 shows vertical cross sections for a transect over 33° N (the black line oriented west–east in the lower-left panel of Figure 19), which begins in the south-central Mediterranean Sea and ends at the eastern border of Iran. This cross section is most relevant for the "jet streak emerges" milestone (Section 4.2.1.3) through the end of the spread phase (Section 4.2.2.2), and the main pattern of interest is the synoptic-scale cyclone that affects the Mediterranean coast. On 24 July, the cyclone entered the domain as strong winds aloft; and by 25 July, the cyclone was vertically stacked at the eastern end of the Mediterranean Sea. At this time, anomalies of warm and dry air also appeared at lower levels over Southwest Asia ahead of the cyclone. However, on 26 July, the strong winds aloft began to split into two distinct maxima: one at upper levels that backtracked slightly westward and one at lower-to-mid levels that shifted eastward into Southwest Asia. The lower-level warm anomaly also shifted eastward at this time. By 27 July, the lower-to-mid level wind maxima seemed to transfer momentum downward and eastward into a narrow jet of strong winds at about 850 hPa, around the longitude of Baghdad (44°–45° E). This was accompanied by a congealing of the warm anomaly into a narrow plume a bit farther east. Finally, the wind jet lifted upward over the next couple of days, while the plume of warm air remained in the same region.

Figure 20. Vertical cross sections of different atmospheric variables at 33° N (see the west–east transect in the bottom-left panel of Fig. 19): anomalies of (*left*) wind speed (in m s^{-1}), (*middle*) air temperature (in degrees Celsius), and (*right*) relative humidity (in percentage points). The anomalies are calculated with respect to the "control" conditions (0000 UTC on 18 July 2018). The *dotted blue vertical line* represents the eastern coast of the Mediterranean Sea, and the *dotted red vertical line* represents the longitude of the cross section shown in Fig. 21. *Top to bottom*: Snapshots at 0000 UTC from 22 to 29 July.

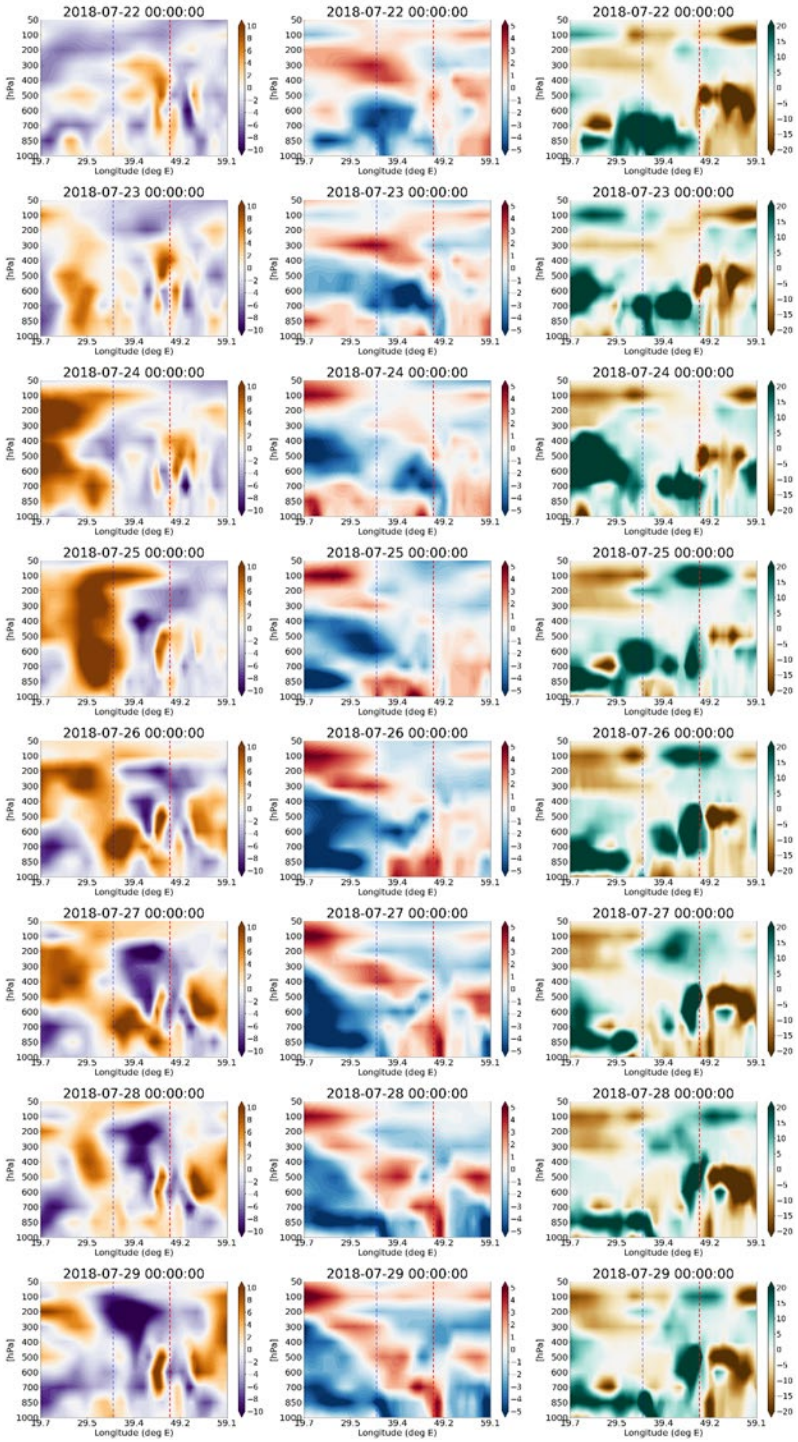

These plumes reappear in Figure 21, which shows vertical cross sections for a transect over 47° E (the black line oriented north–south in the lower-left panel of Figure 19). This transect begins just west of the Caspian Sea, crosses the Arabian Peninsula, and ends in Somalia (south of the Gulf of Aden). This cross section is most relevant for the "arrival at Southwest Asia" milestone (Section 4.2.1.5) through the beginning of the drift phase (Section 4.2.2.4). The first plume to appear in these vertical cross sections is that of temperature: a warm anomaly emerged on 26 July near the surface at about 32° N. On the following day (27 July), a strong low-level pulse of wind appeared between 20° and 30° N, and the plume of warm air expanded southward to 25° N, rising slightly to midlevels of the atmosphere. On 28 July, the core of the wind jet reached its maximum extent, with positive anomalies greater than 10 m s^{-1}, extending almost the entire aforementioned latitudinal range. By this date, another interesting phenomenon emerged: a plume of dry air emerged at about 30° N and steadily extended southward (to about 23° N) and upward (to about 600 hPa). This plume of dry air was nearly collocated with the plume of warm air, and both patterns seemed to "override" the wind jet, perhaps forcing it to the south. Aside from the wind jet moving slightly southward, these dry, warm, and windy anomalies persisted at roughly the same locations and slowly waned in intensity over the next several days.

The meteorological mechanisms behind this dust storm—including the dry, warm, and windy anomalies mentioned above—are a bit unclear. One potential explanation for these anomalies is that they are associated with occlusion, in which warm, dry air is lifted above cooler near-surface air, perhaps near the low-pressure area over the southeastern Arabian Peninsula. It is also possible that the Somali Jet (defined in Section 4.2.2.2) influenced atmospheric dynamics and, therefore, the dust storm over the Arabian Peninsula. Additionally, though Southwest Asia frequently experiences shamal wind patterns, the synoptic-scale setup for shamal occurrence at this time of year typically involves a high-pressure system over the eastern Mediterranean Sea and a low-pressure system over Iran (Yu et al. 2016), neither of which is readily evident for this case study. Finally, some of the authors of this study who have operational forecasting experience in Southwest Asia note that upper-level flow is often cut off or stalls due to downstream blocking, most often resulting in cold air deposition to lower levels and cold air advection near the surface, potentially initiating dust storms.

Figure 21. Same as Fig. 20, except taken over 47° E (see the north–south transect shown in the bottom-left panel of Fig. 19). The *dotted red vertical line* represents the latitude of the cross section shown in Fig. 20, and the *dotted blue vertical line* represents the northern coast of the Gulf of Aden. *Top to bottom*: Snapshots at 0000 UTC from 25 July to 1 August.

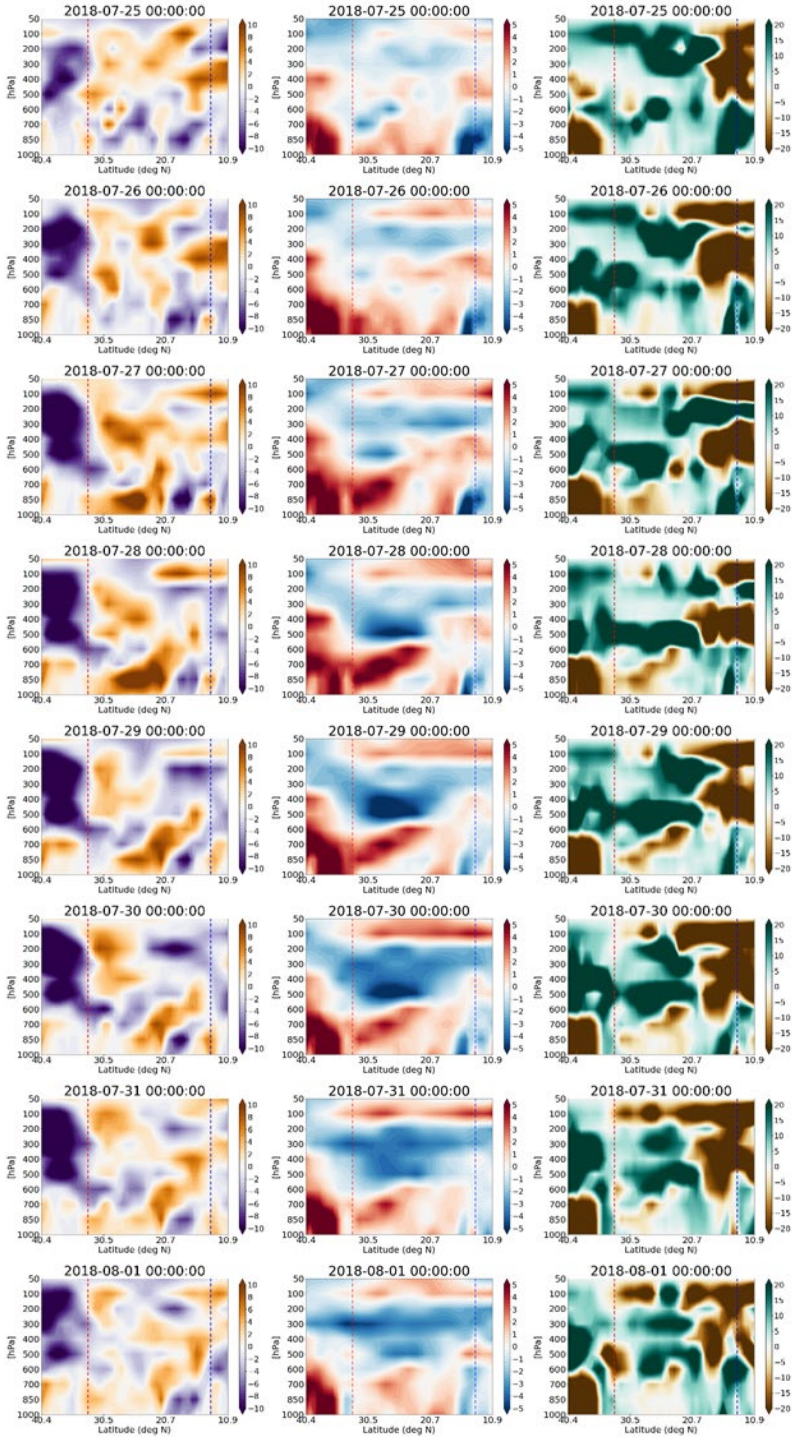

Though upper-level flow did stall before the initiation of this dust storm, the resulting temperature anomalies at lower levels seemed to be warmer than usual, which contrasts this common forecasting scenario. Thus, the dust storm analyzed in this report may be a bit of an edge case. Though it began with a common synoptic-scale setup and encountered typical, shamal-like winds, some of the developments over the course of its evolution were rather unusual when paired with the other large-scale meteorological conditions.

5 Mesoscale Meteorological Analyses

5.1 Precipitation

An important meteorological question regarding this dust storm is whether it was influenced more by synoptic-scale factors (described in previous sections) or by convective activity on *mesoscales* (i.e., length scales between 2 and 2,000 km). To better determine the influence of mesoscale features on the evolution of the dust storm, this section begins with an investigation of precipitation, since convective storms can serve as triggers for dust storms (e.g., Nickling and Brazel 1984). Precipitation data are drawn from two sources—daily data from the CPC Global Unified Gauge-Based Analysis of Daily Precipitation and 3-hourly analyses of precipitation observations assimilated by LIS (see Section 2.2.5 for details).

According to the CPC data, the only dates on which precipitation greater than 1 kg m^{-2} (approximately 1 mm) was detected over the southeastern portion of the Arabian Peninsula were 30–31 July (Figure 22) and 2–3 August. Similarly, the LIS data show notable precipitation in this region on only 31 July (Figure 23) and 1–3 August. For both CPC and LIS, the precipitation was somewhat scattered on these dates and mainly occurred after the dust storm had already traversed the peninsula for multiple days. Thus, it seems unlikely that precipitation in the Arabian Peninsula was a driving factor for this particular dust storm.

Figure 22. An analysis of daily precipitation from the CPC dataset for (*left*) 30 July 2018 and (*right*) 31 July 2018.

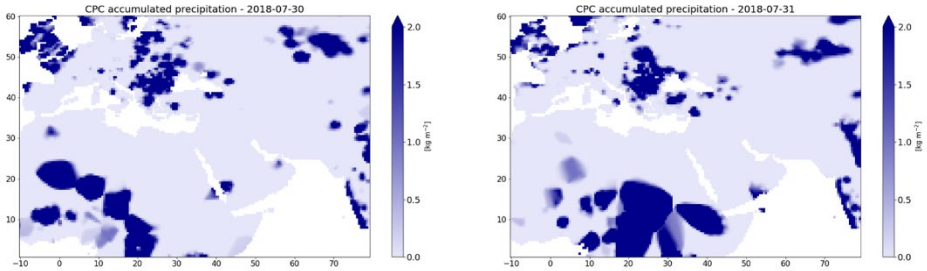

Figure 23. An analysis of precipitation from the LIS dataset for (*left*) 30 July 2018 and (*right*) 31 July 2018. LIS precipitation is accumulated over a 3-hour period ending at 1800 UTC on each of the analyzed days. Note that the scale bar differs between this figure and Fig. 22.

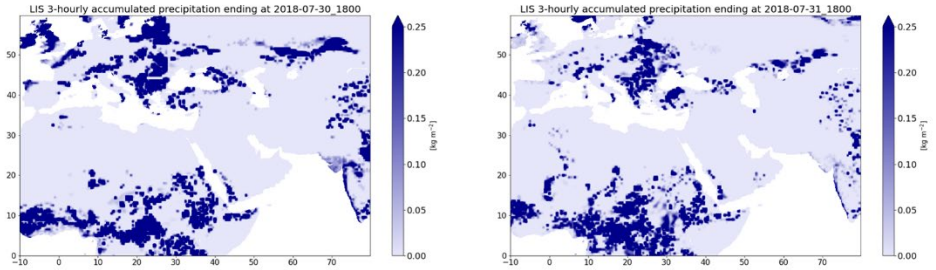

5.2 Convection

Two competing factors dominated the convective environment while the dust cloud was over the southeastern portion of the Arabian Peninsula. On one hand, the atmosphere in the area was primed for precipitation. For example, radiosonde data from Abu Dhabi International Airport in the United Arab Emirates indicated extremely high values of convective available potential energy (CAPE; above 2,500 J kg^{-1}) from 1200 UTC on 31 July to 1200 UTC on 2 August, with an extraordinarily high maximum value of 6,835 J kg^{-1} at 1200 UTC on 1 August. On the other hand, convective inhibition (CIN, also known as the *cap*) was also quite strong during these times, ranging from 385 to 567 J kg^{-1}, which generally prevented the occurrence of deep convective events in the area.

This dichotomy in convective parameters is a result of the extreme difference in meteorological characteristics between the moist, near-surface cool air that originates from the Persian Gulf and the hot, dry air higher in the atmosphere that is characteristic of the Arabian Peninsula. This manifests as a sharp temperature inversion and a similarly sharp drop-off in moisture less than 1 km above the ground. For example, at 0000 UTC on 1 August at Abu Dhabi International Airport, air temperature actually increased from 32.2°C at the surface to 36.2°C at 925 hPa (643 m above ground level), and the dewpoint temperature plummeted from 28.3°C at the surface to 5.2°C at 925 hPa (Figure 24). In particular, the pronounced temperature inversion created a very strong cap for convection at this location, producing a CIN value of 517 J kg^{-1}. Thus, even though the convective environment *near* the surface was ideal for moist convection, the unfavorable convective environment *above* the surface prevented most of it from actualizing.

Figure 24. A Skew-T plot produced from a radiosonde launch at 0000 UTC on 1 August 2018 at Abu Dhabi International Airport in the United Arab Emirates (the *orange square* in Fig. 1). (Image created at University of Wyoming, n.d.)

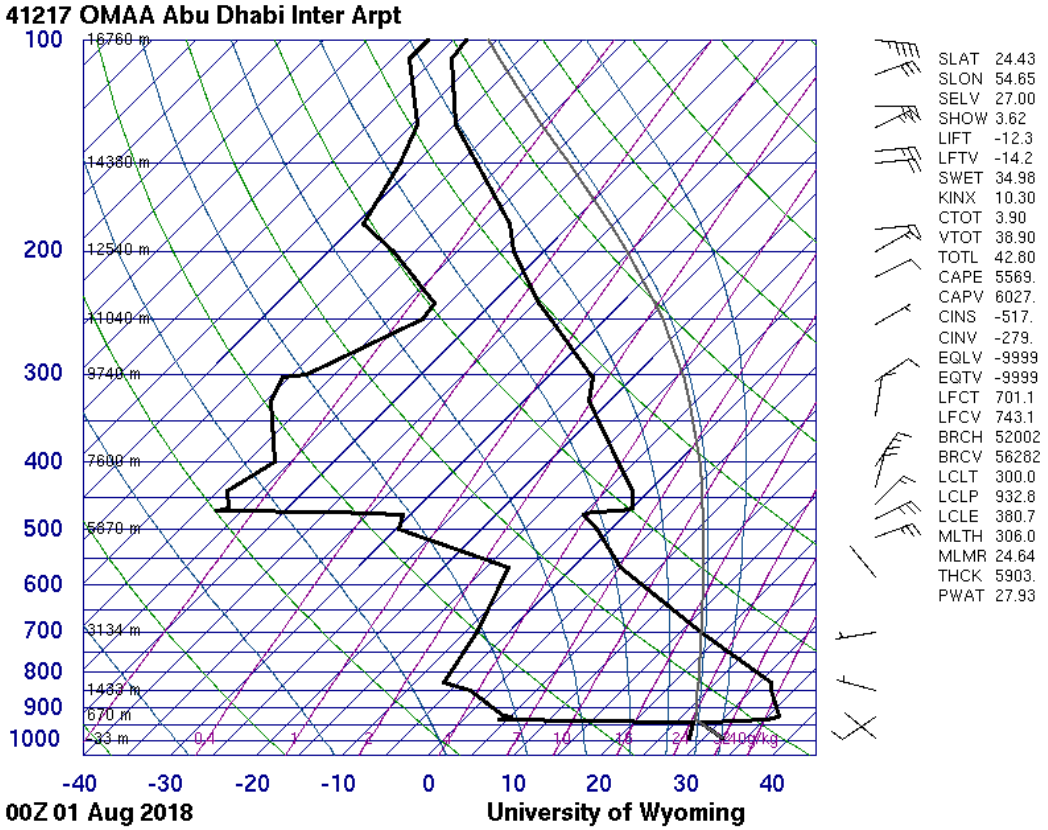

However, some convective activity did occur in the southeastern portion of the Arabian Peninsula at the same time as the dust cloud. Looking at a composite satellite image using the Dust RGB filter from EUMETSAT (Roesli 2018), the dust cloud is visible in purple, pink, and magenta wrapping around the thermal low over the southeastern portion of the Arabian Peninsula (Figure 25). As the day progressed on 30 July, four distinct areas of convective clouds and precipitation popped up along the boundaries of the dust cloud.

While the convection to the northeast of the dust cloud was likely influenced by the Al-Hajar Mountains, sea-breeze dynamics (caused by the interaction of land-based and oceanic air masses), or both, the other areas of convection may have been initiated by either the boundary of the dust cloud itself or the low-pressure area around which it was spinning. If the low-pressure area was the main trigger for convection, then the rising air near its center likely caused enough uplift to generate convective activity. On the other hand, it is possible that temperature or moisture gradients or

both along the boundary of the dust cloud itself served as a “front” to cause uplift and convective activity.

Figure 25. A composite satellite image taken at 1345 UTC on 30 July 2018 using the Dust RGB filter from EUMETSAT (adapted from Roesli 2018). The legend represents categories described in Fuell (2020). Note the areas of convective activity around the dust cloud, which is located over the southeastern portion of the Arabian Peninsula.

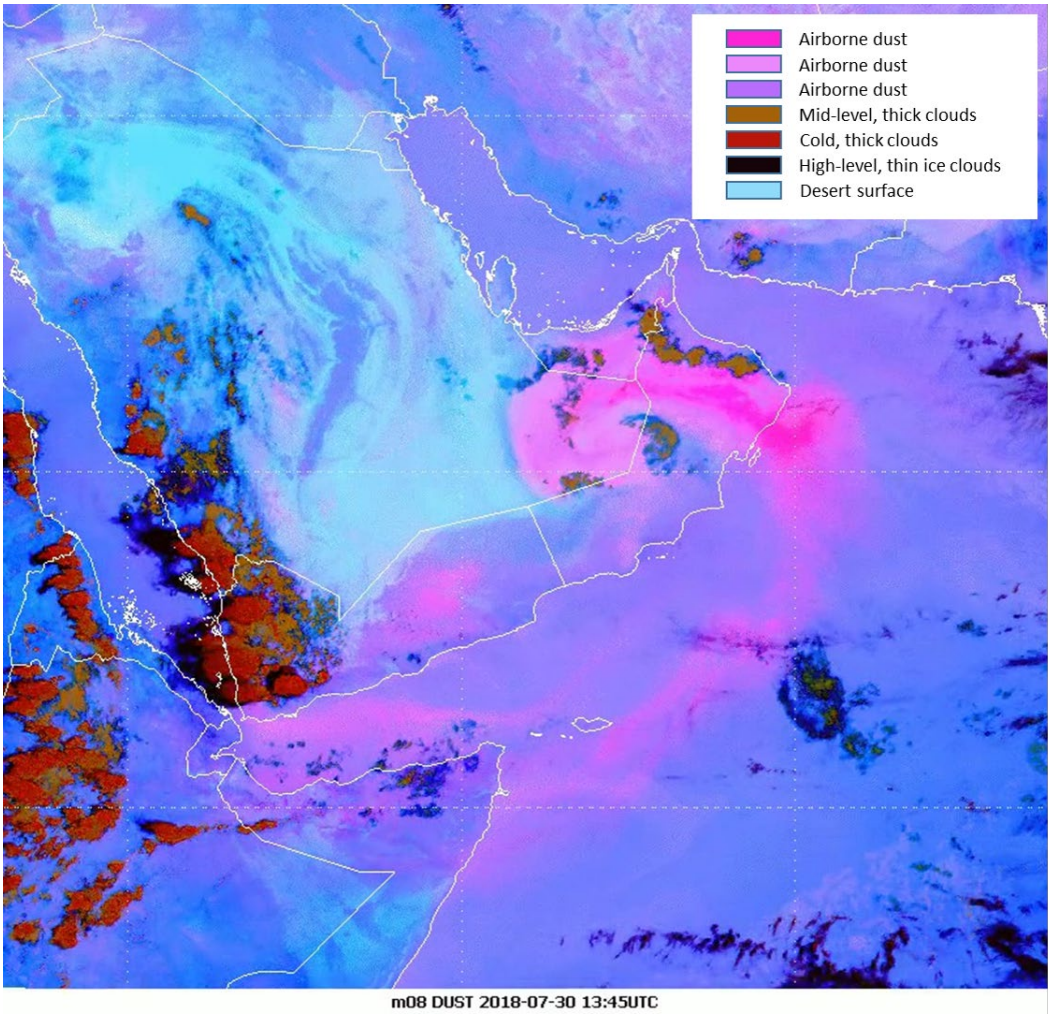

However, the intensity of these convective areas seems to be rather muted, especially compared to the strong convection taking place over the mountains along the western coast of the Arabian Peninsula (Figure 25). Possible reasons include (1) the radiosonde launch at Abu Dhabi from just before this satellite image (Figure 26) indicates far less CAPE than was evident at the later time of Figure 24 (356 vs. 5,569 J kg^{-1}), which would have greatly reduced the potential for strong convective activity, and (2) the locations of the nonorographic convective areas are further inland from the

Persian Gulf and the Arabian Sea (Figure 25), which likely reduced near-surface moisture and, subsequently, values of CAPE.

Figure 26. A Skew-T plot produced from a radiosonde launch at 1200 UTC on 30 July 2018 at Abu Dhabi International Airport in the United Arab Emirates (the *orange square* in Fig. 1). (Image created at University of Wyoming, n.d.)

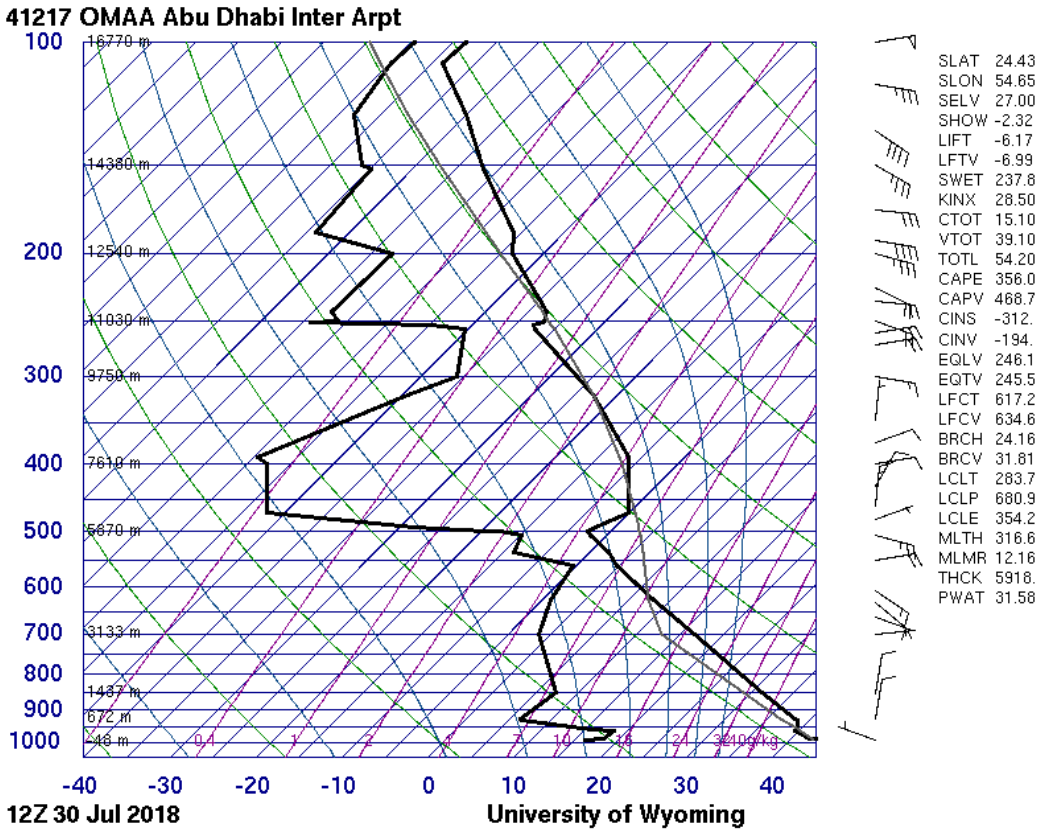

6 Discussion

Given the results described above, it seems unlikely that the initiation, trajectory, and intensity of the dust cloud was influenced by mesoscale convective activity over the Arabian Peninsula. First, the dust cloud had already propagated from Mesopotamia to the southeastern end of the Arabian Peninsula before precipitation even materialized. Second, convection in the area was rather limited while the dust cloud was present, and it may have even been initiated in part by feedbacks related to the dust storm itself (Francis et al. 2021). Therefore, convective activity (e.g., thunderstorms) was likely not the cause of this particular event.

Instead, synoptic-scale activity seems to have played a major role in the development of the dust storm. It is likely that the synoptic-scale system that entered Southwest Asia created a mesoscale warm anomaly over Mesopotamia that may have triggered the dust storm, guided its trajectory over the Arabian Peninsula, and potentially catalyzed the development of a small low-pressure area over the southeastern corner of the peninsula.

Another meteorological mechanism that seems to have played an important role in the dust-storm evolution is *cyclogenesis*, the process by which cyclones develop in the atmosphere. In particular, the synoptic system that arrived at Southwest Asia was likely associated with a mature cyclone (mentioned in Section 4.2.1.5), and cyclogenesis also occurred over the southeastern end of the Arabian Peninsula while the dust storm was present. The cyclone over the Arabian Peninsula may have been caused in part by radiative effects from the dust storm itself (Francis et al. 2021), which adds a degree of complexity to the interactions of the dust storm with its environment.

In fact, the complex interactions between the dust storm and the cyclone over the Arabian Peninsula imply that there are likely multiple scales, direct effects, and indirect effects that are important regarding the dust storm's development. While Francis et al. (2021) describe many of these interactions in detail, it was difficult to diagnose interscale, direct, and indirect interactions in this study because of the lack of atmospheric soundings in the region and the generally coarser resolutions of the products that we analyzed. This provides an opportunity for future studies to investigate these interlinking scales and radiative effects, not only for this dust storm but also for others in Southwest Asia.

7 Conclusions and Recommendations

This report analyzed meteorological conditions that preceded and coincided with the evolution of a major dust storm in Southwest Asia during July–August 2018. After analyzing data from a variety of observation-based sources, this report concludes that the dust storm was initially caused by a synoptic-scale—rather than mesoscale—meteorological system (i.e., a cyclone). However, cascading effects from this synoptic-scale system to the lower troposphere seem to have produced a mesoscale warm anomaly that may have guided the evolution of the dust storm. Additionally, it is likely that other complex interactions between the dust storm and its environment over the Arabian Peninsula contributed to the development of a smaller cyclone in the area, which may have triggered limited convective activity.

This analysis has complicated implications for numerical modeling of this dust storm in Southwest Asia. Because convective activity does not seem to be substantially linked to the initiation or progression of this dust storm, one might initially think that future model simulations of this event need not incorporate nested domains with convection-permitting horizontal resolutions (≤4 km). However, the transition of the synoptic system to a mesoscale pulse upon entering Southwest Asia, along with the radiative effects and mesoscale cyclogenesis associated with the dust storm over the southeastern Arabian Peninsula (Francis et al. 2021), indicate that finer-scale radiative effects and interactions across length scales can be important factors for dust storms in this area. That said, the products we used in this study were generally too coarse of a horizontal resolution to accurately identify these complex meteorological phenomena. Therefore, while most of the effects covered in this report may be resolvable using coarser-resolution model domains, it may be important that future model simulations of this storm and others in the region use convection-permitting horizontal resolutions to ensure that finer-scale meteorological phenomena are not overlooked.

Future work with finer-resolution products and model simulations could focus on untangling several areas of meteorological complexity:

1. Better understanding interactions between the Somali Jet, synoptic-scale and mesoscale cyclogenesis, and the ridge over western Iran that blocked the initial Mediterranean system from entering Southwest Asia

2. Identifying whether there were effects on dust-storm development from topographical features such as the Himalayas and Tibetan Plateau
3. Understanding the general interplay between larger-scale meteorological forcings and smaller-scale radiative, convective, and dynamical features

Obtaining a better understanding of these larger-scale features and their interactions with smaller-scale features may help to better inform forecasts of dust-storm (and thunderstorm) development. One possible application of this information could be "adaptive" forecast systems, in which meteorological model parameters are tuned and ensemble members are weighted midforecast to adjust to changing meteorological forcings. Alternatively, it may be possible to use this information to parameterize multiscale approaches in coarser-resolution model simulations to allow for greater computational efficiency. Either way, obtaining a better understanding of these complex meteorological interactions could ultimately increase predictive capabilities for dust storms such as this one.

Though the results and conclusions presented above are specific to this single dust storm, there is a possibility that they could shed light on other dust storms that occurred in the past (especially during the summer) and improve the prediction of those that will occur in the future.

References

American Meteorological Society. 2017. "Geopotential." Glossary of Meteorology. Last modified 14 November 2017. http://glossary.ametsoc.org/wiki/Geopotential.

Arizona Emergency Information Network. 2019. "Dust Storms." Arizona Emergency Information Network. Accessed 5 February 2021. https://ein.az.gov/hazards/dust-storms.

Dee, D. P., S. M. Uppala, A. J. Simmons, P. Berrisford, P. Poli, S. Kobayashi, U. Andrae, et al. 2011. "The ERA-Interim Reanalysis: Configuration and Performance of the Data Assimilation System." *Quarterly Journal of the Royal Meteorological Society* 137 (656): 553–597. https://doi.org/10.1002/qj.828.

ECMWF (European Centre for Medium-Range Weather Forecasts). 2012. *ERA-Interim Project, Single Parameter 6-Hourly Surface Analysis and Surface Forecast Time Series*. Boulder, CO: Research Data Archive at the National Center for Atmospheric Research, Computational and Information Systems Laboratory. https://doi.org/10.5065/D64747WN.

ECMWF (European Centre for Medium-Range Weather Forecasts). 2019. *ERA5 Reanalysis (0.25 Degree Latitude-Longitude Grid)*. Boulder, CO: Research Data Archive at the National Center for Atmospheric Research, Computational and Information Systems Laboratory. Accessed 8 July 2020. https://doi.org/10.5065/BH6N-5N20.

ECMWF (European Centre for Medium-Range Weather Forecasts). 2020a. "ERA5." ECMWF. https://www.ecmwf.int/en/forecasts/datasets/reanalysis-datasets/era5.

ECMWF (European Centre for Medium-Range Weather Forecasts). 2020b. "ERA-Interim." ECMWF. https://www.ecmwf.int/en/forecasts/datasets/reanalysis-datasets/era-interim.

EUMETSAT. 2022. "Meteosat 0 Degree RGB Composites." EUMETSAT. https://eumetview.eumetsat.int/static-images/MSG/RGB/.

EUMETSAT. n.d. "SEVIRI." EUMETSAT. Accessed 22 August 2022. https://www.eumetsat.int/seviri.

EUMETSAT. n.d. "0 Degree Service." EUMETSAT. Accessed 22 August 2022. https://www.eumetsat.int/0-degree-service.

Federal Aviation Administration. 2020. "ENR 5.7 Potential Flight Hazards." In *Aeronautical Information Publication (AIP)*. 26th ed. Washington, DC: Federal Aviation Administration. Accessed 5 February 2021. https://www.faa.gov/air_traffic/publications/atpubs/aip_html/part2_enr_section_5.7.html.

Francis, D., J.-P. Chaboureau, N. Nelli, J. Cuesta, N. Alshamsi, M. Temimi, O. Pauluis, and L. Xue. 2021. "Summertime Dust Storms over the Arabian Peninsula and Impacts on Radiation, Circulation, Cloud Development and Rain." *Atmospheric Research* 250:105364. https://doi.org/https://doi.org/10.1016/j.atmosres.2020.105364.

Fuell, K. 2020. *GOES-R Dust RGB Quick Guide*. NASA Short-Term Prediction Research and Transition Center (SPoRT). https://weather.msfc.nasa.gov/sport/training/quickGuides/rgb/QuickGuide_DustRGB_GOESR_NASA_SPoRT.pdf.

Giannadaki, D., A. Pozzer, and J. Lelieveld. 2014. "Modeled Global Effects of Airborne Desert Dust on Air Quality and Premature Mortality." *Atmospheric Chemistry and Physics* 14 (2): 957–968. https://doi.org/10.5194/acp-14-957-2014.

Google. 2020. Google Earth Pro. v.7.3.3.7721.

Google. 2022. Google Maps. Accessed 26 May 2022. https://www.google.com/maps.

Hersbach, H., B. Bell, P. Berrisford, S. Hirahara, A. Horányi, J. Muñoz-Sabater, J. Nicolas, et al. 2020. "The ERA5 Global Reanalysis." *Quarterly Journal of the Royal Meteorological Society* 146 (730): 1999–2049. https://doi.org/10.1002/qj.3803.

Johnson, B. T., M. E. Brooks, D. Walters, S. Woodward, S. Christopher, and K. Schepanski. 2011. "Assessment of the Met Office Dust Forecast Model Using Observations from the GERBILS Campaign." *Quarterly Journal of the Royal Meteorological Society* 137 (658): 1131–1148. https://doi.org/10.1002/qj.736.

Kok, J. F., S. Albani, N. M. Mahowald, and D. S. Ward. 2014. "An Improved Dust Emission Model – Part 2: Evaluation in the Community Earth System Model, with Implications for the Use of Dust Source Functions." *Atmospheric Chemistry and Physics* 14: 13043–13061, https://doi.org/10.5194/acp-14-13043-2014.

Kok, J. F., N. M. Mahowald, G. Fratini, J. A. Gillies, M. Ishizuka, J. F. Leys, M. Mikami, et al. 2014. "An Improved Dust Emission Model – Part 1: Model Description and Comparison Against Measurements." *Atmospheric Chemistry and Physics* 14:13023–13041. https://doi.org/10.5194/acp-14-13023-2014.

Kumar, S. V., C. D. Peters-Lidard, Y. Tian, P. R. Houser, J. Geiger, S. Olden, L. Lighty, et al. 2006. "Land Information System: An Interoperable Framework for High Resolution Land Surface Modeling." *Environmental Modelling & Software* 21 (10): 1402–1415. https://doi.org/10.1016/j.envsoft.2005.07.004.

LeGrand, S. L., C. Polashenski, T. W. Letcher, G. A. Creighton, S. E. Peckham, and J. D. Cetola. 2019. "The AFWA Dust Emission Scheme for the GOCART Aerosol Model in WRF-Chem v3.8.1." *Geoscientific Model Development* 12 (1): 131–166. https://doi.org/10.5194/gmd-12-131-2019.

Liu, M., D. L. Westphal, A. L. Walker, T. R. Holt, K. A. Richardson, and S. D. Miller. 2007. "COAMPS Real-Time Dust Storm Forecasting during Operation Iraqi Freedom." *Weather and Forecasting* 22 (1): 192–206, https://doi.org/10.1175/WAF971.1.

Ma, S., X. Zhang, C. Gao, D. Q. Tong, A. Xiu, G. Wu, X. Cao, et al. 2019. "Multimodel Simulations of a Springtime Dust Storm over Northeastern China: Implications of an Evaluation of Four Commonly Used Air Quality Models (CMAQ v5.2.1, CAMx v6.50, CHIMERE v2017r4, and WRF-Chem v3.9.1)." *Geoscientific Model Development* 12 (11): 4603–4625, https://doi.org/10.5194/gmd-12-4603-2019.

Maricopa County. 2021. "Dust Storms." Maricopa County, Arizona. Accessed 5 February 2021. https://www.maricopa.gov/5557/Monsoon#dust.

McDonald, E. V., S. N. Bacon, S. D. Bassett, R. Amit, Y. Enzel, T. B. Minor, K. McGwire, O. Crouvi, and Y. Nahmias. 2016. *Integrated Terrain Forecasting for Military Operations in Deserts: Geologic Basis for Rapid Predictive Mapping of Soils and Terrain Features*. New York, NY: Springer New York.

Nickling, W. G., and A. J. Brazel. 1984. "Temporal and Spatial Characteristics of Arizona Dust Storms (1965–1980)." *Journal of Climatology* 4 (6): 645–660. https://doi.org/10.1002/joc.3370040608.

NOAA PSL (National Oceanic and Atmospheric Administration Physical Sciences Laboratory). 2020. "CPC Global Unified Gauge-Based Analysis of Daily Precipitation." Boulder, CO: NOAA PSL. https://psl.noaa.gov/data/gridded/data.cpc.globalprecip.html.

Roesli, H.-P. 2018. "Dense Dust Outbreak across the Arabian Peninsula: Summer Shamal Pushed Dense Dust across the Arabian Peninsula to Its South Coast and out over the Arabian Sea in Late July/Early August 2018." EUMETSAT, https://www.eumetsat.int/dense-dust-outbreak-across-arabian-peninsula.

Sissakian, V. K., N. Al-Ansari, and S. Knutsson. 2013. "Sand and Dust Storm Events in Iraq." *Natural Science* 5 (10): 1084–1094. https://doi.org/10.4236/ns.2013.510133.

Terradellas, E., S. Nickovic, and X.-Y. Zhang. 2015. "Airborne Dust: A Hazard to Human Health, Environment and Society." *WMO Bulletin* 64 (2): 42–46. https://public.wmo.int/en/resources/bulletin/airborne-dust-hazard-human-health-environment-and-society.

University of Wyoming. n.d. "Atmospheric Soundings." University of Wyoming, College of Engineering, Department of Atmospheric Science. Accessed 1 July 2020. http://weather.uwyo.edu/upperair/sounding.html.

Weather Underground. 2020. "Historical Weather." Weather Underground. https://www.wunderground.com/history.

Yu, Y., M. Notaro, O. V. Kalashnikova, and M. J. Garay. 2016. "Climatology of Summer Shamal Wind in the Middle East." *Journal of Geophysical Research: Atmospheres* 121 (1): 289–305. https://doi.org/10.1002/2015jd024063.

Abbreviations

AOD	Aerosol optical depth
CAPE	Convective available potential energy
CIN	Convective inhibition
CPC	Climate Prediction Center
ECMWF	European Centre for Medium-Range Weather Forecasts
ERA-Interim	ECMWF Reanalysis Interim
ERA5	ECMWF Reanalysis version 5
EUMETSAT	European Organisation for the Exploitation of Meteorological Satellites
GP	Geopotential
LIS	Land Information System
MSLP	Mean sea-level pressure
OMAA	Abu Dhabi International Airport
SEVIRI	Spinning Enhanced Visible and InfraRed Imager

REPORT DOCUMENTATION PAGE

Form Approved
OMB No. 0704-0188

1. REPORT DATE (DD-MM-YYYY)	2. REPORT TYPE	3. DATES COVERED (From - To)
November 2022	Technical Report / Final	FY19–FY20

4. TITLE AND SUBTITLE
Meteorological Influences of a Major Dust Storm in Southwest Asia during July–August 2018

5a. CONTRACT NUMBER

5b. GRANT NUMBER

5c. PROGRAM ELEMENT
0603734A

6. AUTHOR(S)
Ross E. Alter, Sandra L. LeGrand, Freddie D. Spates, William D. Ledbetter, Sherman D. Minnigan, John W. Thompson, Kindra I. Carter, and Phillip D. Elliott

5d. PROJECT NUMBER
T15

5e. TASK NUMBER

5f. WORK UNIT NUMBER

7. PERFORMING ORGANIZATION NAME(S) AND ADDRESS(ES)

US Army Engineer Research and Development Center (ERDC)
Cold Regions Research and Engineering Laboratory (CRREL)
72 Lyme Road, Hanover, NH 03755

US Air Force
28th Operational Weather Squadron
Shaw Air Force Base, SC 29152

ERDC Geospatial Research Laboratory (GRL)
7701 Telegraph Road, Alexandria, VA 22315-3864

8. PERFORMING ORGANIZATION REPORT NUMBER
ERDC TR-22-22

9. SPONSORING / MONITORING AGENCY NAME(S) AND ADDRESS(ES)
Headquarters, US Army Corps of Engineers
Washington, DC 20314-1000

10. SPONSOR/MONITOR'S ACRONYM(S)
USACE

11. SPONSOR/MONITOR'S REPORT NUMBER(S)

12. DISTRIBUTION / AVAILABILITY STATEMENT
Approved for public release; distribution is unlimited.

13. SUPPLEMENTARY NOTES

14. ABSTRACT

Dust storms can be hazardous for aviation, military activities, and respiratory health and can occur on a wide variety of spatiotemporal scales with little to no warning. To properly forecast these storms, a comprehensive understanding of the meteorological dynamics that control their evolution is a prerequisite. To that end, we chose a major dust storm that occurred in Southwest Asia during July–August 2018 and conducted an observation-based analysis of the meteorological conditions that influenced the storm's evolution. We found that the main impetus behind the dust storm was a large-scale meteorological system (i.e., a cyclone) that affected Southwest Asia. It seems that cascading effects from this system produced a smaller, near-surface warm anomaly in Mesopotamia that may have triggered the dust storm, guided its trajectory over the Arabian Peninsula, and potentially catalyzed the development of a small low-pressure system over the southeastern end of the peninsula. This low-pressure system may have contributed to some convective activity over the same region. This type of analysis may provide important information about large-scale meteorological forcings for not only this particular dust storm but also for future dust storms in Southwest Asia and other regions of the world.

15. SUBJECT TERMS
Dust storms--Middle East, Dust control, Meteorology, Weather forecasting--Mathematical models, Remote sensing, Satellites

16. SECURITY CLASSIFICATION OF:			17. LIMITATION OF ABSTRACT	18. NUMBER OF PAGES	19a. NAME OF RESPONSIBLE PERSON
a. REPORT	b. ABSTRACT	c. THIS PAGE			19b. TELEPHONE NUMBER (include area code)
Unclassified	Unclassified	Unclassified	SAR	58	